

CHARACTERIZING RATE INHIBITION IN H₂O/H₂ GASIFICATION VIA MEASUREMENT OF ADSORBED HYDROGEN CONCENTRATION

M. G. Lussier, Z. Zhang, and D. J. Miller

Department of Chemical Engineering
Michigan State University
East Lansing, MI 48824

Keywords: Gasification, Kinetics, Rate Inhibition

INTRODUCTION

Gasification of coal for fuels production is not currently used on a wide scale because extreme conditions are needed to achieve reasonably fast reaction rates. One reason for these extreme conditions is the inhibition of gasification by hydrogen in the reacting gas phase. For example, gasification rate decreases by an order of magnitude with the addition of only 1 ppm hydrogen to steam [1], and rate has been shown to decline significantly with conversion in hydrogen and steam/hydrogen mixtures [2,3]. Hydrogen dissociatively chemisorbed onto carbon is very stable, generally accepted as dissociative in nature, and requires temperatures approaching 1800 K to completely desorb [4].

The three possible modes of hydrogen inhibition in steam gasification are as follows [3]:



Selection of any of the possible inhibition modes gives the following basic rate expression [3,5]:

$$\text{rate}_{\text{co}} = \frac{C_A K_1 P_w}{1 + K_2 P_w + K_3 P_H^n} \quad (4)$$

Dissociative adsorption gives a value of 0.5 for n [3], which has been found to be the case for low hydrogen pressures [6] and subatmospheric steam pressures [7]. Reverse oxygen exchange and associative hydrogen adsorption both give values of one for n , as reported in earlier studies [5,8,9]. Associative adsorption has been found to contribute to inhibition at higher pressures, but dissociatively bound hydrogen still dominates char surfaces [10].

EXPERIMENTAL

A char of Dow Saran Resin (MA 127) was prepared in a quartz tube reactor at 1173 K in flowing nitrogen for 0.5 hr., ground and sieved to -60+100 mesh, then annealed in an alumina reactor at 5 K/min to 1773 K in flowing argon for 6 hr.

Chars were gasified inside a quartz lined Inconel 625 differential packed bed microreactor which was housed inside a larger pressure vessel capable of simultaneous operation at 1273 K and 6.6 MPa. The entire system was designed to have absolute minimal internal volume to facilitate accurate measurement of transient species. After gasification in 40% steam and various proportions of argon and hydrogen at 1123 K and pressures ranging from 0.3 to 3.3 MPa, rapid switching to pure argon was done and transients monitored. The inherent system transient response was accounted for by using 1% krypton as a tracer in the reactant gas argon.

After gasification, chars were removed, weighed, and placed inside the alumina reactor for temperature programmed desorption (TPD) to measure the quantity of adsorbed hydrogen. Samples were outgassed in argon at 10 K/min to 1773 K in a Mellen split tube furnace with a programmable temperature controller. Effluent species from both reactors were analyzed with an Ametek M100M Quadrupole Mass Spectrometer, which is interfaced with a personal computer for data collection and deconvolution.

RESULTS

Figures 1 and 2 show rate curves for steam/hydrogen gasification of annealed Saran char at 1.0 MPa and 3.1 MPa total pressure, 1123 K, 40% steam, and varying concentrations

of hydrogen balanced with argon. The CO + CO₂ formation rate is independent of steam partial pressure at these conditions when no hydrogen is present in the reactant gas, and hydrogen inhibition of CO + CO₂ formation is clearly observable with increasing hydrogen partial pressure. Methane formation rate is approximately first order in hydrogen partial pressure and independent of steam partial pressure. A decline in rate is also observed over the first 1% conversion when hydrogen is present in the reactant gas for both CO + CO₂ formation and methane formation; this decline becomes more pronounced under higher hydrogen partial pressures. In the most extreme case, CO + CO₂ formation rate approaches zero at 1.0 MPa total pressure and 0.6 MPa hydrogen partial pressure. All rate curves gradually increase with conversion after the first 1%, which follows the increase in char surface area. Figure 3 shows char surface areas as determined by N₂ BET analysis, indicating a very highly porous material is formed with conversion.

Figure 4 shows adsorbed hydrogen on a per unit weight basis as a function of char conversion following gasification. Surprisingly, adsorbed hydrogen concentration is only a function of conversion and not reactant gas composition. There appears to be two zones of adsorption behavior. The first is an initial rapid adsorption to almost 30 ccH₂(STP)/g up to 1% conversion, and the second is a more gradual but steady increase in adsorbed hydrogen to 100 ccH₂/g at 70% conversion. The hydrogen peak maximum is at 1500 K during TPD, indicating that hydrogen is dissociatively adsorbed on the char surface.

Figure 5 shows adsorbed hydrogen concentration following gasification on a per unit area basis. The increase in adsorbed hydrogen with conversion after the initial rapid adsorption stage is partially accounted for by the increase in char surface area with conversion; however, the gradual increase in adsorbed hydrogen concentration per unit area indicates that hydrogen continues to adsorb onto the char throughout the entire course of gasification.

Figure 6 shows CO + CO₂ formation rate during a reaction in which hydrogen fraction of the reactant gas is cycled between 0% and 60%. A rate curve from a steam only gasification has been included for reference. Rate reversibly changes from a value close to that of the reference curve to a very low value as hydrogen is added and excluded from the reactant gas. This indicates that steady state rate is only a function of reactant gas composition.

DISCUSSION

Our results support both reverse oxygen exchange and dissociative hydrogen adsorption as modes of inhibition in steam/hydrogen gasification of chars, with reverse oxygen exchange acting throughout the course of reaction and dissociative hydrogen adsorption inhibiting rate only upon initial exposure to hydrogen. Temperature programmed desorption studies show that dissociative hydrogen adsorption occurs throughout gasification, most rapidly during the first 1% conversion. There may be a relationship between this initial rapid adsorption and the rate decline over the same initial 1% conversion for chars exposed to hydrogen-containing reactant gases; however, the same initial rapid hydrogen adsorption is not accompanied by a decline in rate when there is no hydrogen present in the reactant gas. Conversion beyond the first 1% is also marked by an increase in adsorbed hydrogen, albeit much less rapidly, but not by a decline in rate. Step changes in reactant gas compositions result in gasification rates that reach steady-states which are similar to those achieved with unchanging reactant gas compositions.

This leads to the conclusion that, at high conversions (>1%) the adsorbing hydrogen does not compete for the same active sites at which gasification occurs. If the dissociative hydrogen adsorption measured by TPD has blocked sites active in gasification, the increase in surface hydrogen concentration would lead to a corresponding decrease in the total number of active sites and thus a decrease in gasification rate regardless of reactant gas composition. This does not occur.

At low conversion, however, dissociative hydrogen adsorption may play a role. At high hydrogen partial pressures, reverse oxygen exchange cannot be solely responsible for hydrogen inhibition because it is driven by hydrogen partial pressure which is not changing during the initial rapid decline in rate. It appears that dissociative hydrogen adsorption contributes to rate inhibition by competing with oxygen exchange for active sites. Upon initial exposure of the char to a reactant gas with a high hydrogen partial pressure, a greater proportion of active sites become blocked with dissociatively adsorbed hydrogen over the course of 1% conversion. Once the rapid transient adsorption is complete, an

equilibrium is established in which there are fewer active sites and steady-state rate is achieved.

The fact that methane formation rate is approximately first order in hydrogen partial pressure may appear to be contradictory to a reduction in the number of active sites upon an increase in hydrogen partial pressure; however, the mode by which methane is formed makes a higher steady state rate with fewer active sites possible. Both CO + CO₂ and methane formation rates decrease simultaneously over 1% conversion upon exposure of chars to hydrogen, indicating that sites active for both must be affected. Unlike oxygen exchange, methane formation must be preceded by hydrogen adsorption, so an unsaturated carbon site is not always needed to form methane. Oxidation does require an unsaturated site, of which there are fewer under higher hydrogen partial pressure.

Our findings lead us to conclude that annealed Saran char is covered with two types of active sites. The most abundant are those that acquire dissociatively adsorbed hydrogen from the gas phase to cover much of the char surface, achieving a bulk H/C ratio as high as 0.1 at about 70% conversion. The second type of sites are active for gasification, with competition between oxidation and methane formation reactions. Under low hydrogen partial pressure the driving force for reverse oxygen exchange is small, as is the driving force for methane formation. Thus, C(O) formation at active sites dominates and CO is the primary product, with CO₂ subsequently formed via the shift reaction. As hydrogen partial pressure is increased the case is reversed. The reverse oxygen exchange driving force is increased as is methane formation. The total number of unsaturated surface carbons is reduced over 1% conversion by adsorbing hydrogen until an equilibrium is reached with active site competition. Methane formation includes hydrogen adsorption onto the char surface, while oxygen exchange requires unsaturated active sites. The oxygen exchange reaction will always have to compete with the methane formation reaction for unsaturated active sites, while the methane formation reaction does not have to compete with the oxygen exchange reaction since methane formation can occur at sites that have been saturated with hydrogen.

CONCLUSIONS

Reverse oxygen exchange and dissociative hydrogen adsorption both inhibit steam gasification of annealed Saran char, which is covered with two major types of active sites. The first and most abundant type of site dissociatively adsorbs hydrogen throughout the course of reaction, and is inactive for gasification. The second type of site is active in gasification to form CO and methane, but can become blocked with dissociatively adsorbed hydrogen upon exposure to increased hydrogen partial pressure. Reverse oxygen exchange, however, always influences CO formation. The total concentration of sites which are active towards gasification, as well as the equilibrium at these sites between oxidation, methane formation, and site blockage determines char gasification rate.

ACKNOWLEDGMENT

The support of the United States Department of Energy (UCR Program) through Grant # DE-FG22-93PC93213 is gratefully acknowledged.

REFERENCES

1. Montet, G.L. and Myers, G.E., Carbon **9**, 673 (1971).
2. Toomajian, M.E., Lussier, M.G., and Miller, D.J., Fuel **71**, 1055 (1992).
3. Huttinger, K.J. and Merdes, W.F., Carbon **30**(6), 883 (1992).
4. Redmond, J.P. and Walker, P.L.Jr., J. Phys. Chem. **64**, 1093 (1960).
5. Gadsby, J., Hinshelwood, C.N., and Sykes, K.W., Proc. Royal Soc. London **A187**, 129 (1946).
6. Giberson, R.C. and Walker, J.P., Carbon **3**, 521 (1966).
7. Yang, R.T. and Duan, R.Z., Carbon **23**(3), 325 (1985).
8. Blackwood, D.J. and McGrory, F., Aust. J. Chem. **11**, 16 (1958).
9. Mims, C.A. and Pabst, J.K., ACS Div. Fuel Chem. Prepr. **25**(3), 263 (1980).
10. Huttinger, K.J., Carbon **26**(1), 79 (1988).

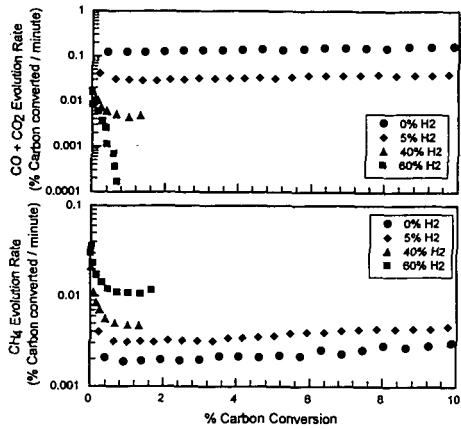


Figure 1: H₂O/H₂ Gasification Rate of Annealed Saran Char at 1.0 MPa

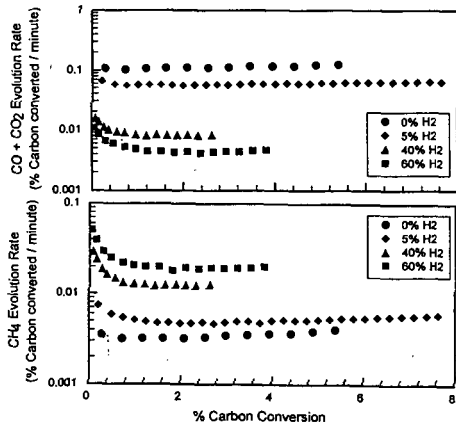


Figure 2: H₂O/H₂ Gasification Rate of Annealed Saran Char at 3.1 MPa

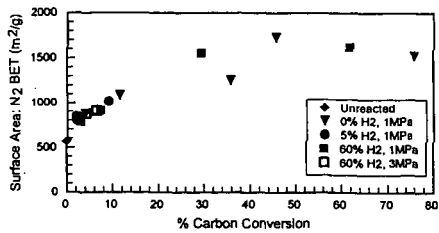


Figure 3: Surface Area (N₂ BET) of Annealed Saran Char Following H₂O/H₂ Gasification

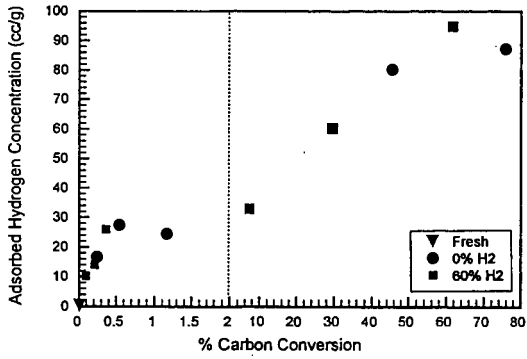


Figure 4: Adsorbed Hydrogen Concentration per Unit Weight on Annealed Saran Char Following H₂O/H₂ Gasification at 1.0 MPa

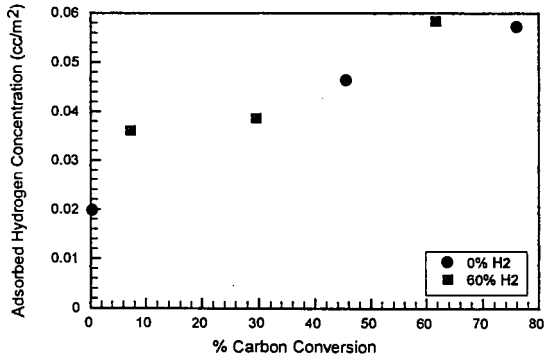


Figure 5: Adsorbed Hydrogen Concentration per Unit Surface Area on Annealed Saran Char Following H₂O/H₂ Gasification at 1.0 MPa

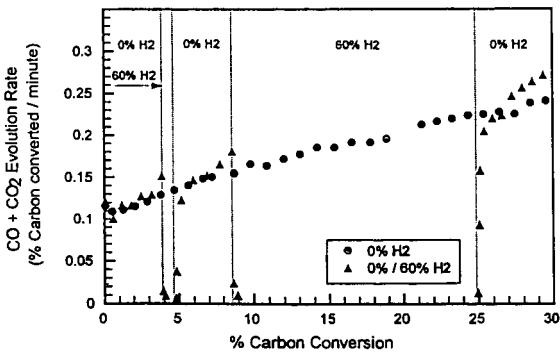


Figure 6: H₂O/H₂ Gasification Rate of Annealed Saran Char at 1.0 MPa, Step Changes in Reactant Gas Composition

THE ROLE OF SUBSTITUTIONAL BORON IN CARBON OXIDATION: INHIBITOR AND CATALYST

M. Karra, P. A. Thrower and L. R. Radovic

Fuel Science Program

Department of Materials Science and Engineering
The Pennsylvania State University, University Park, PA 16802

KEYWORDS: carbon oxidation, inhibition, catalysis, boron.

INTRODUCTION

Carbon oxidation has been very thoroughly investigated. It is a reasonably well understood heterogeneous gas/solid reaction [1-4]. Yet there are many practical and fundamental 'details' that need to be sorted out. There are also some very important fundamental issues that are not understood. Others may want to add (or subtract?) some issues, but here is our list of key outstanding questions in the C/O₂ reaction:

- (a) What is the exact nature of the relation between 'reactive' C(O) intermediates and 'stable' C-O complexes on the carbon surface?
- (b) What is the reason for the commonly observed "compensation effect" in both uncatalyzed and catalyzed carbon gasification?
- (c) Which structural features of the carbon surface govern the magnitude of the CO/CO₂ ratio in the products of oxidation and, in particular, how is CO₂ formed?
- (d) Is it possible that, when carbon is doped with boron, both a catalytic and an inhibiting effect can be observed?

A companion paper presented at this symposium [5] addresses issue (c). The present communication deals with issue (d). Reference 6 had roughly the same title as this paper, but it ended with a question mark. In the macroscopic world, in contrast to the quantum world [7], mutually exclusive phenomena are not commonly thought to coexist. So boron is considered to be either an inhibitor or a catalyst of carbon oxidation, but not both. Here we provide additional arguments for this remarkable influence of boron on the oxidation of a wide range of carbonaceous solids (and we thus replace the question mark with an exclamation point). Elsewhere [7] we address issues (a) and (b); in particular we argue that both the elusive concept of the compensation effect and the intriguing balance between reactive and stable carbon-oxygen surface complexes may have an analogous explanation to the one offered here for the role of boron in carbon oxidation.

Boron is considered to be one of the very few promising candidates for chemical protection of carbon/carbon composite materials against oxidation. Oxidation protection is of paramount importance for the use of these strategic materials in demanding (e.g., structural) aerospace applications. (Most ceramic coatings have a thermal expansion mismatch with carbon and thus develop cracks which lead to carbon exposure to high-temperature O₂.) The conventional wisdom is that boron inhibits carbon oxidation. Its inhibiting effect can be manifested in three different ways: (a) Substitutional boron enhances the graphitization of carbon [8-10]. (b) As the surface carbon atoms are consumed, substitutional boron forms an oxide surface film, which acts as an O₂ diffusion barrier and an active site blocker [9,11-14]. (c) Substitutional boron redistributes the π electrons in the basal plane (graphene layer), lowers the Fermi level of carbon, and hence presumably inhibits the desorption of CO and CO₂ [9,11,14]. This last mode of inhibition is of great fundamental interest; it had not been verified in the past. As a consequence of our recent results [6], and upon closer examination of some early studies, its closer scrutiny is warranted. We provide such a scrutiny in the present communication.

EXPERIMENTAL

Three widely differing carbon materials were used: a heat-treated ('graphitized') carbon black (Graphon, Cabot Corp.), Saran char (produced by pyrolysis of a PVC/PVDC copolymer manufactured by Dow Chemical Co.) and a glassy carbon (a phenolic-resin-derived material, Alfa-Aesar). Boron was introduced substitutionally into the quasi-graphitic lattice by heating these carbons, physically mixed with boron powder (99.999%, Alfa-Aesar) at different levels (1, 2 and 5 wt % B), to ~2450 °C in Ar [6,15]. Some loss of boron occurred during this treatment (see Results).

Isothermal carbon oxidation experiments (~10 mg samples; 1 atm; 21% dry O₂, 99.994%; 250 cc/min) were performed with these samples in a Mettler TGA. The reaction temperature was achieved after heating the sample in N₂ at 25 °C/min; negligible gasification occurred during this nonisothermal period [15]. In selected cases, the reactive surface area (RSA) [16] of the carbons was determined using a commercial transient kinetics apparatus (SSITKA 2000, Altamira Instruments). The

integrated area under the transient decay curves for CO and CO₂, after switching from O₂ to inert gas at different conversion levels, was used as a first approximation to true RSA values.

RESULTS

Figure 1 shows that boron acts as a catalyst of oxidation of glassy carbon. Figure 2 summarizes the kinetic data (at the same carbon conversion level) for the boron-doped polymer-derived carbons. In agreement with the behavior observed for boron-doped Graphon [6], boron is seen to act as a catalyst at low boron loadings and as an inhibitor at higher boron loadings. The global activation energy does not seem to depend in a consistent way on boron content. It is governed rather by the nature of the carbon: as almost invariably reported in the literature, it increases as the degree of crystalline perfection of the carbon increases (33±3 kcal/mol for undoped and boron-doped Saran char vs. 44±5 kcal/mol for undoped and boron-doped Graphon).

Figure 3 shows the x-ray diffraction profiles for undoped and boron-doped Saran chars. At the highest boron loadings, the signature of enhanced graphitization - splitting of the {10} turbostratic peak (at ~43 °2θ) into {100} and {101} graphitic peaks (at ~42 °2θ and ~44 °2θ) - is observed.

Figures 4 and 5 summarize the catalytic and/or inhibiting effects of boron in carbon oxidation as a function of the reaction temperature and the extent of reaction (percent carbon conversion). In agreement with the data shown in Figure 2 and in our earlier work [6], the net effect depends on the concentration of boron in the carbon. It is surprising that boron, present presumably as substituent atoms in the carbon lattice, acts as a catalyst at low loadings and as an inhibitor at higher loadings. This is in contrast to all other reports in the literature [11,12,14], where an inhibiting effect was found at all boron concentration levels when dry O₂ was used as the reactant. Interestingly, Thomas and Roscoe [17] observed a catalytic effect in moist oxygen. More recently, Rodriguez and Baker [18] confirmed the inhibiting effect of the boron oxide, but reported a catalytic effect of boron carbide.

In summary then, all our experimental results obtained to date show that boron inhibits carbon oxidation at high initial boron loadings, high temperatures and high carbon conversion levels. In contrast, boron catalyzes carbon oxidation at low initial loadings, low temperatures and low conversion levels. Additional results [15] suggest that boron is an inhibitor of oxidation at low O₂ partial pressures and a catalyst at higher pressures.

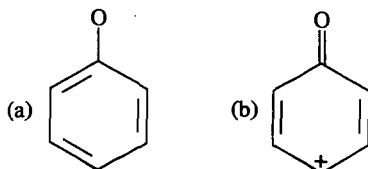
DISCUSSION

In light of the foregoing results, the premises on which some of the earlier work was based [9,11,14] need to be reexamined.

There is no doubt that boron catalyzes the graphitization of a wide range of carbons. (Figure 3 and our other results [15] confirm this well known effect.) This in turn leads in general to a decrease in carbon reactivity [19] and thus, effectively, to oxidation inhibition.

On the basis of results shown in Figures 4 and 5, there is no compelling reason to doubt either that B₂O₃ is formed upon oxidation of boron-doped carbons [17]. It is worth noting, however, the recent work by Cermignani et al. [20] in which X-ray photoelectron spectroscopy was used to identify the boron-containing species after heat treatment and oxidation of boron-doped CVD carbon films. After oxidation at 600 °C for 4 h, they saw no clear evidence that B₂O₃ was the predominant species formed; instead, they identified boron oxycarbides as the dominant surface species.

What needs reevaluation is the proposed [9] electronic effect of boron (mechanism (c) in the Introduction). Its origin lies in the electronic effect of a carbon gasification catalyst which, upon oxygen adsorption, induces type (b) distribution of the π electrons in the graphene layer [21]:



By accepting electrons from the graphene layer (e.g., into unfilled d bands of a transition metal), a catalyst is thought to facilitate both O₂ adsorption (by increasing the C-O bond strength) and product desorption (by weakening the adjoining C-C bonds, as illustrated above).

In contrast to the oxygen-transfer theory [22], the electron-transfer theory of catalysis [23] has not found much support in the carbon gasification literature and had not been confirmed experimentally. Nevertheless, a recent theoretical study of potassium-catalyzed graphite oxidation [24] does indicate that this electron-donating catalyst lowers the work function of graphite and thus enhances the dissociation probability of O₂ on the surface. This is opposite to the well known electronic effect of substitutional boron, which does not contribute electrons to the delocalized π system of the graphene layer and lowers the Fermi level of graphite [12]. Boron would thus be expected to decrease, to some extent at least, the dissociation (chemisorption) probability of O₂. Indeed, Allardice and Walker [12b] concluded that boron inhibits the chemisorption of CO₂ in the C/CO₂ reaction.

This redistribution of π electrons in the presence of substitutional boron results not in the weakening of C-O bonds and strengthening of C-C bonds [9], but in exactly the opposite effect (see figure above): being essentially an electron 'acceptor', as discussed above, boron is predicted to induce type (b) distribution of π electrons and thus weaken C-C bonds and strengthen C-O bonds. This trend was confirmed by a straightforward application of Hückel molecular orbital theory [15]. In fact, Allardice and Walker [12a] used this argument, together with the observed decrease in the activation energy for oxidation of graphite, to anticipate the *catalytic* effect of substitutional boron (even though in their study this effect was masked and overwhelmed by the inhibiting effect of B₂O₃).

Substitutional boron thus emerges as *both* a catalyst and an inhibitor of carbon oxidation. The catalytic effect is clearly observed for the first time; this is attributed to the fact that samples possessing relatively high surface areas were used, and the catalytic effect was not masked by the ubiquitous inhibiting effect of B₂O₃. The fact that boron is a catalyst under conditions favoring desorption control (low temperature and high oxygen partial pressure) and inhibitor under conditions favoring adsorption control (high temperature and low oxygen partial pressure) is quite intriguing. It suggests that this phenomenon is yet another example of the well known 'compensation effect', which we tentatively interpreted [7] as a 'macroscopic complementarity principle': in the presence of substitutional boron the turnover frequency for carbon atom removal increases (due to the catalytic effect of C-C bond weakening), but the number of reactive sites decreases (due to the inhibiting effect on O₂ adsorption). The latter point is illustrated in Figure 6.

ACKNOWLEDGMENTS

This study was made possible by financial support from the U.S. Air Force Office of Scientific Research (AFOSR URI F49620-93-1-0311, Major T. Erstfeld, Project Manager). Fruitful collaboration with G. S. Rellick (The Aerospace Corporation, El Segundo, CA) is also acknowledged. A partial SSITKA equipment grant was received from Altamira Instruments.

REFERENCES

1. R. H. Essenhigh, in "Chemistry of Coal Utilization", 2nd Suppl. Vol. (M. A. Elliott, Ed.), Wiley, New York, 1981, p. 1153.
2. N. M. Laurendeau, *Prog. Energy Combust. Sci.* **4**, 221 (1978).
3. P. L. Walker, Jr., R. L. Taylor and J. M. Ranish, *Carbon* **29**, 411 (1991).
4. J. Lahaye and P. Ehrburger (Eds.), *Fundamental Issues in Control of Carbon Gasification Reactivity*, Kluwer, Dordrecht, The Netherlands, 1991.
5. K. Skokova and L. R. Radovic, this symposium, March 1996.
6. M. Karra, R. J. Zaldivar, G. S. Rellick, P. A. Thrower and L. R. Radovic, in *Proc. 22nd Biennial Conf. Carbon*, San Diego, CA, July 1995, p. 646.
7. L. R. Radovic, M. Karra and K. Skokova, in *Proc. 22nd Biennial Conf. Carbon*, San Diego, CA, 1995, p. 636.
8. S. Marinkovic, C. Suznjevic and I. Dezarov, *Carbon* **7**, 185 (1969).
9. L. E. Jones and P. A. Thrower, *J. Chim. Phys.* **84**, 1431 (1987).
10. R. J. Zaldivar, R. W. Kobayashi and G. S. Rellick, *Carbon* **29**, 1145 (1991).
11. D. W. McKee, in *Chem. Phys. Carbon* (P. A. Thrower, Ed.) **23**, 173 (1991).
12. D. J. Allardice and P. L. Walker, Jr., (a) *Carbon* **8**, 375 (1970); (b) *ibid.* **8**, 773 (1970).
13. P. Ehrburger, P. Baranne and J. Lahaye, *Carbon* **24**, 495 (1986).
14. W. Kowbel, Y. Huang and H. Tsou, *Carbon* **31**, 355 (1993).
15. M. Karra, M. S. Thesis, The Pennsylvania State University, 1996.
16. A. A. Lizzio, H. Jiang and L. R. Radovic, *Carbon* **28**, 7 (1990).
17. J. M. Thomas and C. Roscoe, in *Proc. 2nd Conf. Ind. Carbon Graphite*, London, 1965, p. 249.
18. N. M. Rodriguez and R. T. K. Baker, *J. Mater. Res.* **8**, 1886 (1993).
19. L. R. Radovic, P. L. Walker, Jr. and R. G. Jenkins, *Fuel* **62**, 849 (1983).

20. W. Cermignani, T. E. Paulson, C. Onneby and C. G. Pantano, *Carbon* **33**, 367 (1995).
21. P. L. Walker, Jr., M. Shelef and R. A. Anderson, in *Chem. Phys. Carbon* (P. L. Walker, Jr., Ed.) **4**, 287 (1968).
22. D. W. McKee, in *Chem. Phys. Carbon* (P. L. Walker, Jr. and P. A. Throrer, Eds.) **16**, 1 (1981).
23. T. J. Long and K. W. Sykes, *Proc. Royal Soc. A* **215**, 100 (1952).
24. C. Janiak, R. Hoffmann, P. Sjövall and B. Kasemo, *Langmuir* **9**, 3427 (1993).

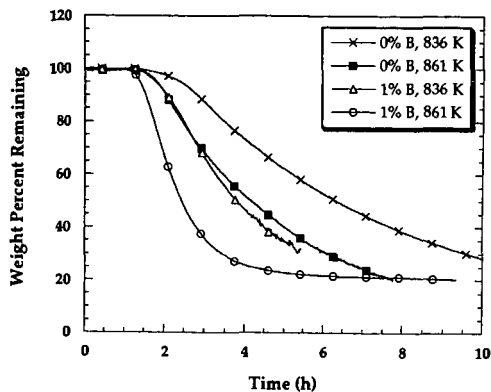


Figure 1. Typical TGA plots for boron-free and boron-doped glassy carbon.

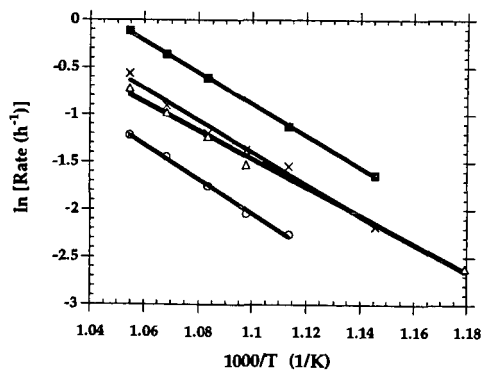


Figure 2. Arrhenius plots for Saran char doped with different amounts of boron and gasified at 1 atm (21% O₂): x, 0% B, 33 kcal/mol; ■, 1.1% B, 33 kcal/mol; Δ, 1.9% B, 30 kcal/mol; ○, 3.8% B, 36 kcal/mol.

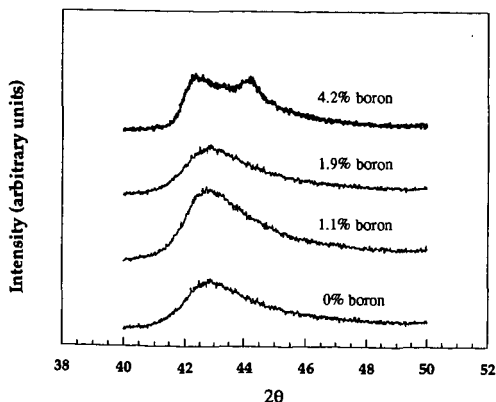


Figure 3. X-ray diffraction patterns for Saran char doped with different concentrations of boron.

LOW TEMPERATURE STEAM-COAL GASIFICATION CATALYSTS

Edwin J. Hippo and Deepak Tandon
Department of Mechanical Engineering and Energy Processes
Southern Illinois University
Carbondale, IL 62901

Keywords: Steam Gasification, Low-Temperature Catalyst, Binary Catalysts.

INTRODUCTION

Shrinking domestic supplies and larger dependence on foreign sources have made an assortment of fossil fuels attractive as possible energy sources. The high sulfur and mineral coals of Illinois would be an ideal candidate as possible gasification feedstock.

Large reserves of coal as fossil fuel source and a projected shortage of natural gas (methane) in the US, have made development of technology for commercial production of high Btu pipeline gases from coal of interest. Several coal gasification processes exist, but incentives remain for the development of processes that would significantly increase efficiency and lower cost. A major problem in coal/char gasification is the heat required which make the process energy intensive. Hence, there is a need for an efficient and thermally neutral gasification process.

At the present time, natural gas (methane) reserves are sufficient to meet the demands but projections indicate a dwindling supply in the future. There is a need to develop an economical process for production of methane to ensure a steady supply. Direct methanation of high sulfur and mineral coals would not only utilize this important fossil fuel feedstock but would also be inexpensive as compared to other energy intensive gasification processes. Direct formation of methane in the gasifier would also increase the efficiency of the combined cycle power generation plant over that of an integrated gasification combined cycle (IGCC) process, producing CO and H₂ only.

Catalytic steam methanation of coal is an almost thermoneutral process:



The role of the catalyst in coal/carbon gasification has been to reduce the reaction temperature and increase the rate of reaction. The main objective of these studies has been to improve the production of water gas, producer gas, or hydrogen as sources for ammonia production. Most of these works were carried out at lower pressures and have little qualitative value in assessing the catalytic effects on coal/char gasification for methane production.

Catalytic gasification of coal/carbon has attracted much attention recently. A majority of the elements in the periodic table have been tested as potential gasification catalysts and a number of leading candidates have been identified. Catalyst that are active at low temperatures would favor the process of direct gasification for methane production, since low temperature and high pressure favors the formation of methane.

Various oxides, halides and carbonates of both alkali and alkaline earth metals, along with transition metals have been surveyed as possible char gasification catalysts. Some of the general conclusions drawn are as follows:

- (1) Catalytic effect decreases with increasing temperature;
- (2) Catalysts are more effective in gasification processes if steam is present in the gasification gases;
- (3) There usually is an optimum catalyst loading, beyond which either negligible or negative effects are observed;
- (4) Relative effects of catalysts can differ under different reaction conditions;
- (5) Gasification reactivity can be effected significantly by the method /condition of catalyst impregnation; and
- (6) Catalyst impregnation is more effective than physical mixing with the carbon.

Methane cannot be produced by the reaction of C(H)₂ complex with hydrogen, if no catalyst is present. Therefore, incentives exist to explore the thermoneutral catalytic steam methanation (reaction 1) of coals to produce methane economically and in a single reaction.

Catalytic effects on gasification of carbon materials have been studied for last several decades. The mechanisms of catalytic gasification are still not completely understood and are not the same for all catalysts systems and reactions. In general, reactivity of catalyzed carbons is at least one order of magnitude higher than those of uncatalyzed carbons. A majority of the elements in the periodic table have been tested as potential gasification catalysts. The main objective of these studies have been to improve the process for production of water gas or producer gas. Outside of the work at Exxon, these work, have little qualitative value in assessing the catalytic effects on coal/char gasification for production of methane from steam.

Thermodynamically, high pressure and low temperature shift the reaction towards methane formation. It was the aim of this research to study the catalytic steam gasification of high sulfur, high mineral, agglomerating coals at elevated pressures and lower temperatures for production of methane. This research focused mainly on prevention of catalyst deactivation and coal char agglomeration. A study of pure catalysts was performed at various temperatures (773 to 973 K) and pressures (0.1 to 3.5 MPa). These catalysts were also used in various combinations to determine any synergistic effects on the methanation reaction. At High pressures alkali metals such as potassium, kept transition metal catalyst(s) reduced, mobile, and activated for longer time periods. The alkali metals and Mo also helped in the penetration of transition metals and thus provided a better contact with the carbon matrix.

The ultimate goal of this research was to develop a low temperature sulfur resistant catalyst system that would not only be efficient and economic but would also produce methane in a single step. The single-reaction process would eliminate the cost of separation, compression and recycling of hydrogen gas. Developing a low temperature catalyst system should also help reduce catalyst recycle costs. At low temperature operations, interaction of catalyst with the coal mineral phases are less likely.

BACKGROUND

The mechanism of gasification is not the same for all the catalysts systems and reactions. The catalyst basically works through a redox cycle, and dissociates molecular oxygen into atomic oxygen much faster than the uncatalyzed carbon surface. It is these mobile oxygen atoms that migrate to the carbon surface, thereby, generating oxides of carbon (CO and CO₂). This effect is called the *Spill-over effect*.

Recently it has been established that oxygen transfer plays a major role in catalysis. For transition metal salts (e.g. Fe, Ni) the catalyst oscillates between two oxidation states, on the other hand alkali metal salts (e.g. Na, K) during catalysis involve a carboxylic, phenolic or a completely reduced structure.

The catalytic effects of a catalyst system depends on; (i) activation of the catalyst, (ii) intrinsic activity of the active species, and (iii) inactivation of the active species [1]. During activation of the catalyst the metal salt reacts and decomposes to the elemental state or any other intermediate state that is catalytic. The dispersion and adhesion of such species on the carbon surface is extremely important. The catalyst loses its activity due to agglomeration, volatilization, inclusion in micropores, poisoning or interaction with the mineral matter of the coal. Catalyst mobility is important for its effectiveness. If the catalyst is in the molten phase, diffusion will depend on the temperature difference between the melting point and gasification temperature [2-5].

Single catalyst (one metal element) gasification has several limitations: (i) the rate of gas production is very slow, (ii) reduced active surface area by pore blockage, (iii) rapid deactivation of the catalyst by poisoning and sintering, (iv) low gas production, (v) loss of contact of catalyst and reactant, and (vi) volatilization of catalyst, and catalyst encapsulation by carbon deposition [6-12].

Exxon catalytic gasification process produces substitute natural gas (SNG) by catalytic steam gasification of coal [13]. The process operates at 700°C and 3.5 MPa and uses potassium carbonate as the catalyst. The catalyst plays three important roles:

- (1) It enhances the rate of gasification and lowers the reaction temperature thereby favoring methane production.
- (2) Favors gas phase methanation equilibrium.
- (3) Inhibition of swelling and caking of coals.

In this process calcium performed better at lower loadings because it does not interact

preferentially with the mineral matter. Since calcium is not as mobile as potassium its impregnation was very critical.

Iron is one of the desired catalysts for steam gasification of coal. The cheap availability of iron and its salts (mainly sulfate) make it even a more promising catalyst than the alkali metals. Commercially, it is one of the best catalysts for about 10 wt.% char conversion. The problem in using iron is that it deactivates (oxidizes) very rapidly. Nickel is another good catalyst, but it also deactivates fast and the gas production stops after about 10% graphite conversion [14]. Calcium deactivates because of sintering as a result of particle growth but remains active for longer burnoff times than iron and nickel. Abel et al. [2] found that reaction rate falls as a result of pore blockage by the catalyst which results in the reduction of accessible surface area. The catalytic activity of iron has been described by various mechanisms: electron transfer, oxygen transfer, carbide mechanism [15-17].

Bimetallic catalysts have addressed some of the limitations of single catalyst gasification. Gas production increases with the use of bimetallic catalyst. The catalyst remains active for a longer duration and is more resistant to poisoning. A catalyst that is not deactivated by sulfur would enable the gasification of high sulfur coals. Synergistic effects have been observed by the use of bimetallic catalysts [18].

Bimetallic catalysts not only increase the activity and selectivity towards desired products, but are also more resistant towards catalyst deactivation by poisoning or carbon deposition. Researchers have performed both experimental and theoretical analysis for bimetallic catalyst systems and have found significant differences in the surface and bulk compositions, as a result of one component of the catalyst system segregating preferentially to the surface. Also, an adjuvant gas can influence the segregation process [19-20].

EXPERIMENT

The coal used in this study was IL. No. 6 coal. This coal was selected because of its high sulfur content. Both the raw and demineralized coal samples were gasified in this study. Gasification of all samples was conducted in an electric furnace. The reactor, was a stainless steel tube, mounted vertically in the furnace. A high pressure pump was employed to pump water at the rates of 30 ml hr⁻¹ gm⁻¹ of coal. All the experiments were performed at 500 and 700°C and 500 and 1000 psig. Samples were placed in the reactor in a wire mesh bucket. The glass wool at the top of the reactor was used to trap any tarry material that might tend to escape. The system was purged with argon and pressurized with steam. Gas samples were collected at regular time intervals (5, 15, 30, and 60, min.) in gas bags and gas chromatography was performed on each gas bag. Product gas composition and concentration were monitored by gas chromatography. From the gas yield and composition, the carbon conversion in each interval and the accumulated carbon conversion were calculated. The experiments were terminated when the rate of gas production diminished significantly.

RESULTS AND DISCUSSION

At 500°C and both 500 and 1000 psig, negligible amount of raw coal was gasified. This suggested that the activation energy barrier cannot be crossed at 500°C for the raw coal alone. The unreacted steam would condense at the bottom of the reactor. Even when the flow rate of water was reduced to 0.25 ml min⁻¹ similar problems were encountered. At 700°C there was a substantial increase in the amount of coal gasified. Almost 36-39 wt.% (assuming 100% carbon) coal was gasified at 500 psig. At 5 minutes the analysis of the gas at 500 psig showed CO₂ as the main gas (77%), there was significant amount of CH₄ (18%) and minute quantities of CO and H₂. Gas production was observed till 15 minutes but at this time CO₂ was the primary gas (89%). No gas production was observed at 30 minutes. At 700°C and 1000 psig there was a slight increase in the amount of coal gasified (43 wt.%). The gas analysis at 5 min showed 61% CO₂, 28% CH₄, 5% H₂, and 6% CO. At 15 min the gas composition was 79% CO₂, 16% CH₄, 3% H₂, and 2% CO. Once again no gas production was observed at 30 min. This high jump in coal conversion at 700°C suggested that at this temperature the energy was sufficient to clear the activation barrier and a portion of the char formed was also gasified. Demineralized coal gasified almost like raw coal with 38 wt.% conversion at 700°C and 500 psig. The gas analysis at 5 min showed 88% CO₂, 0% CH₄, 6% H₂, and 6% CO. At 15 min the gas composition was 96% CO₂, 0% CH₄,

4% H₂, and 0% CO. Once again no gas production was observed at 30 min. Conversion numbers and gas analyses are presented in Table 1.

In presence of the catalyst significant gasification was observed at 500°C and 500 psig. Both the raw and demineralized coal samples were gasified in presence of the catalyst. Catalysts studied thus far are salts of potassium, iron, nickel, and molybdenum. For the single catalyst experiments of potassium salts (hydroxide and carbonate) increasing the catalyst loading from 5 to 10% had little effect on coal conversion. For KOH catalyzed raw coal experiments the coal conversion was around 28-35 wt.%. Similarly increase in temperature had very little effect on conversion. Gas production was observed till 30 min. Increase in pressure resulted in increased methane formation. For 10% potassium loading (KOH) the gas analysis at 5 min showed 55% CO₂, 32% CH₄, 7% H₂, and 6% CO. At 15 min the gas composition was 61% CO₂, 29% CH₄, 6% H₂, and 4% CO. At 30 min the gas composition was 66% CO₂, 26% CH₄, 5% H₂, and 3% CO. No gas production was observed at 45 min. For potassium carbonate, however, the conversion went down from 40 to 33% with increase in the loading from 5 to 10%. This could be due to interaction of potassium carbonate with the mineral of coal at higher loadings. The gas analyses were comparable to the KOH experiments. Conversion numbers and gas analyses are presented in Table 1.

Salts of transition metals behaved like potassium salts. The conversion numbers were comparable but the methane concentration was slightly lower. In some cases the gas production stopped after 15 min. At 500°C and 500 psig almost 30% conversion was achieved with 10% loading of iron chloride. The gas analysis at 5 min showed 64% CO₂, 27% CH₄, 5% H₂, and 4% CO. At 15 min the gas composition was 68% CO₂, 26% CH₄, 5% H₂, and 1% CO. At 30 min the gas composition was 74% CO₂, 23% CH₄, 3% H₂, and 0% CO. No gas production was observed at 45 min. At the same conditions 37% conversion was achieved with nickel hydroxide. The gas analysis at 5 min showed 59% CO₂, 30% CH₄, 7% H₂, and 4% CO. At 15 min the gas composition was 67% CO₂, 26% CH₄, 5% H₂, and 2% CO. At 30 min the gas composition was 72% CO₂, 24% CH₄, 4% H₂, and 0% CO. No gas production was observed at 45 min. Conversion with molybdenum oxide was lower (22%) under same conditions. No gas production was observed after 15 min. The conversion numbers and the gas analyses for the demineralized coal samples were comparable to the raw coal conversions. Conversion numbers and gas analyses are presented in Table 1.

When potassium hydroxide was used with transition metals significant increases in the conversions were obtained and also the concentration of the methane in the product gas increased substantially. As shown in Table 1 at 500°C and 500 psig when iron chloride and potassium hydroxide are used together at 5% each loading the conversion increased to 42% with an increase in methane concentration in the product gas. The gas analysis at 5 min showed 56% CO₂, 35% CH₄, 7% H₂, and 2% CO. At 15 min the gas composition was 59% CO₂, 34% CH₄, 6% H₂, and 1% CO. At 30 min the gas composition was 69% CO₂, 27% CH₄, 4% H₂, and 0% CO. No gas production was observed at 45 min. At 10% each loading the conversion went up to 53%. The gas analysis at 5 min showed 47% CO₂, 39% CH₄, 9% H₂, and 5% CO. At 15 min the gas composition was 52% CO₂, 37% CH₄, 7% H₂, and 4% CO. At 30 min the gas composition was 58% CO₂, 33% CH₄, 6% H₂, and 3% CO. No significant gas production was observed at 45 min. This shows some synergistic effects. Possibly potassium helps keep iron reduced for longer duration and thus the conversion and methane formations are increased. Conversion numbers and gas analyses are presented in Table 1.

When nickel hydroxide and potassium hydroxide are used together at 500°C and 500 psig and at 5% each loading the conversion was 39%. The gas analysis at 5 min showed 60% CO₂, 33% CH₄, 5% H₂, and 2% CO. At 15 min the gas composition was 69% CO₂, 27% CH₄, 3% H₂, and 4% CO. No significant gas production was observed at 30 min. At 10% each loading the conversion went up to 55%. The gas analysis at 5 min showed 58% CO₂, 35% CH₄, 7% H₂, and 0% CO. At 15 min the gas composition was 67% CO₂, 28% CH₄, 5% H₂, and 0% CO. At 30 min the gas composition was 76% CO₂, 21% CH₄, 3% H₂, and 0% CO. No significant gas production was observed at 45 min. At 700°C and 1000 psig and 5% each loading of nickel and potassium a conversion of 74% was achieved. The gas had increased concentration of carbon monoxide and lower methane production. Experiments performed with demineralized coal samples resulted in slightly lower conversions but similar gas analyses.

CONCLUSIONS

1. Significant amounts of hydrogen can be produced at moderate gasification conditions.
2. Low to negligible CO concentrations and ratios of H₂/CO is at synthesis gas stoichiometry.
3. Steam reforming of methane is avoided at 3-6 MPa range.
4. The combination of alkali and transition metals gave significant synergistic effects.

Table 1.
Carbon Conversion and Gas Analyses of Various Steam-Coal Gasification Experiments

Run	Temp (°C)	Pres (psig)	Catalyst	Loading (Wt.%)	Conv. %	H ₂ /CO ₂ / CH ₄ /CO 5 Min	H ₂ /CO ₂ / CH ₄ /CO 15 Min	H ₂ /CO ₂ / CH ₄ /CO 30 Min
Raw	700	500	None	None	37	2/77/18/3	1/89/8/2	-----
Raw	700	500	None	None	39	2/76/18/4	0/91/7/2	-----
Raw	700	500	None	None	36			
Raw	700	1000	None	None	43	5/61/28/6	3/79/16/2	-----
Demin	700	500	None	None	38	6/88/0/6	4/96/0/0	-----
Raw	700	500	K ₂ CO ₃	5	36.4			
Raw	700	1000	K ₂ CO ₃	5	39.9	6/53/35/6	5/59/32/4	4/68/26/2
Raw	700	1000	K ₂ CO ₃	10	33.1	7/54/32/7	5/66/26/3	-----
Raw	500	500	KOH	10	28.4	7/55/32/6	6/61/29/4	5/66/26/3
Raw	500	1000	KOH	10	36.4	6/52/35/7	5/59/31/5	4/64/28/4
Raw	700	750	OH	5	34.6	7/54/33/6	5/60/30/5	5/65/26/4
Raw	500	500	KOH	10	28.4	7/55/32/6	6/61/29/4	5/66/26/3
Raw	500	500	FeCl ₂	10	29.7	5/64/27/4	5/68/26/1	3/74/23/0
Raw	500	500	KOH/FeCl ₂	5 each	42.16	7/56/35/2	6/59/34/1	4/69/27/0
Raw	500	500	KOH/FeCl ₂	10 each	53	9/47/39/5	7/52/37/4	6/58/33/3
Raw	500	1000	NiOH	10	37	7/59/30/4	5/67/26/2	4/72/24/0
Raw	700	1000	KOH/NiOH	5 each	74	8/53/32/7	4/82/11/3	4/72/24/0
Raw	500	500	KOH/NiOH	10 each	55	7/58/35/0	5/67/28/0	3/76/21/0
Raw	500	500	KOH/NiOH	5 each	39	5/60/33/2	3/69/27/1	-----
Raw	500	500	MoO ₃	10	22	1/71/28/0	0/83/17/0	-----

ACKNOWLEDGMENTS

This work was supported by a grant supplied by the New Energy Development Organization (NEDO) through the International Cooperative Research Program of Japan. Coal samples were provided by the Illinois Basin Coal Sample Program (IBCSP) which is maintained by the Illinois State Geological Survey.

REFERENCES

1. J. Alder, K.J. Huttinger, and R. Minges, *Fuel*, **63**, 1397, 1984.
2. D.A. Fox and A.H. White, *Ind. Eng. Chem.*, **23**, 259, 1931.
3. D.W. McKee and D. Chatterji, *Carbon*, **13**, 381, 1975.
4. D.W. McKee and D. Chatterji, *Carbon*, **16**, 53, 1976.
5. T. Wigmans, H. Haringa, and J.A. Moulijn, *Fuel*, **62**, 185, 1983.
6. J. Carrazza, W.T. Tysoe, H. Heinemann and G.A. Somorjai, *J. Catal.*, **96**, 234, 1985.
7. J.S. Binford and H. Eyring, *J. Am. Chem. Soc.*, **60**, 486, 1956.
8. R.G. Jenkins, S.P. Nandi, and P.L. Walker, Jr. *Fuel*, **52**, 288, 1973.
9. E.J. Hippo and P.L. Walker, Jr., *Fuel*, **54**, 245, 1974.
10. K.J. Huttinger and W.F. Merdes, *Carbon*, **30**(6), 883, 1992.
11. J.L. Johnson, *Fuel Chem. Div. Prepr.*, 170th ACS national meeting, Chicago, IL, Aug. 24-29, 1975.
12. J.W. Patrick and F.H. Shaw, *Fuel*, **51**, 69, 1972.
13. W.R. Epperly and H.M. Siegel, *Proc. of the 11th Intersociety Energy Conversion Conference*, Nevada, USA, 1976.
14. T. Wigmans, A. Hoogland, P. Tromp, and J.A. Moulijn, *Carbon* **21**(1) 13, 1983.
15. F.W. Long and K.W. Sykes, *J. Chem. Phys.*, **47**, 361, 1950.
16. Y. Tamai, H. Watanabe, and A. Tomita, *Carbon*, **12**, 453, 1974.
17. W.L. Holstein and M. Boudart, *Fuel*, **62**, 162, 1983.
18. Y. Nishiyama, *Fuel Processing Technology*, **29**, 31, 1991.
19. V. Ponec, *Surf. Sci.*, **80**, 352, 1979.
20. M.F.L. Johnson and V.M.J. Leroy, *J. Catal.*, **35**, 434, 1974.

CATALYSIS OF PETROLEUM COKE GASIFICATION
BY CALCIUM HYDROXIDE AND CARBONATE

Yasuo Ohtsuka, Atsuko Yamauchi and Qianlin Zhuang
Research Center for Carbonaceous Resources
Institute for Chemical Reaction Science, Tohoku University
Sendai 980-77, Japan

Keywords: Gasification, Petroleum coke, Calcium catalyst

ABSTRACT

Catalysis of petroleum coke gasification in pure CO_2 by $\text{Ca}(\text{OH})_2$ or CaCO_3 has been investigated with a thermobalance. The reactivity of the original coke is very low. $\text{Ca}(\text{OH})_2$ kneaded with the carbon in water enhances the reactivity drastically, and thus realizes complete gasification at 900°C within 25 min. CaCO_3 shows almost the same catalytic activity as $\text{Ca}(\text{OH})_2$ except for the initial stage of gasification. The X-ray diffraction measurements and X-ray photoelectron spectroscopy of partly gasified samples reveal that the calcium promotes remarkably the formation of non-crystalline carbon, in other words, surface oxygen complexes, during gasification. The temperature programmed desorption shows that there are strong interactions between calcium and carbon, which contributes to the creation of reactive sites.

1. INTRODUCTION

Petroleum coke as a byproduct in coking processes of residual oils is used partly as an energy source [1]. Since it is composed of graphitized carbon, however, the gasification reactivity is low compared with coal. It may be interesting from a practical point of view if the reactivity is enhanced by catalyst addition and consequently petroleum coke can be employed as a feedstock for the production of hydrogen and syngas. However, no successful approach has been reported so far.

In earlier publications we have found that inexpensive $\text{Ca}(\text{OH})_2$ and CaCO_3 are the most promising gasification catalysts [2-4], as long as water slurry of $\text{Ca}(\text{OH})_2$ or CaCO_3 is mixed with low rank coals with large amounts of oxygen functional groups as ion exchangeable sites. Whereas, recent dynamic studies on the catalysis of carbon gasification by Ca have shown that the catalyst can create surface oxygen complexes, that is, reactive sites, even on well-ordered graphite [5,6].

It may be expected from these observations that graphitized carbon in petroleum coke is also activated during gasification by the calcium from $\text{Ca}(\text{OH})_2$ or CaCO_3 . Therefore the present work focuses on making clear catalyst effectiveness of these compounds for the gasification of petroleum coke and on elucidating the catalysis by the calcium.

2. EXPERIMENTAL

Petroleum coke of size fraction 75-150 μm was used. The proximate and ultimate analyses are shown in Table 1. The ash and oxygen contents were very low. The X-ray diffraction (XRD) analysis revealed the presence of graphitized carbon, but the degree of graphitization was not so developed, as shown by the XRD parameters of interplanar spacing (d_{002}) and average crystalline height (L_c) in Table 1. Powdery $\text{Ca}(\text{OH})_2$ or CaCO_3 was loaded onto the carbon by simply kneading them in water, Ca loading in the dried sample being 3 wt% as metal. The $\text{Ca}(\text{OH})_2$ -loaded carbon was used unless otherwise described.

About 20 mg of the sample was heated quickly up to 800 - 1000°C in a stream of pure CO_2 , and the weight loss during the isothermal gasification was monitored with a thermobalance [3,4]. The XRD, X-ray photoelectron spectroscopy (XPS), and temperature programmed desorption (TPD) of partly gasified samples were carried out to characterize the catalyst state and reactive sites. In the TPD runs, the sample after gasification at 850°C followed by cooling to room temperature was heated in He up to 1000°C , and CO and CO_2 released were determined with a gaschromatograph.

3. RESULTS AND DISCUSSION

Rate Enhancement by Calcium Catalyst

The profiles for the CO_2 gasification of petroleum coke are shown in Figure 1, where conversion is calculated on a basis of fixed carbon after devolatilization. The reactivity of the original coke was quite low at 800-900°C, and fixed carbon conversion at 900°C was < 20 wt% after 2 h. On the other hand, $\text{Ca}(\text{OH})_2$ enhanced the reactivity dramatically; the conversion at 800°C reached 65 wt% after 2 h, and at 900°C the carbon was gasified completely within 25 min. Our previous studies have shown that the Ca cations in saturated $\text{Ca}(\text{OH})_2$ solution can readily be ion-exchanged with COOH groups when mixed with low rank coals at room temperature [7], and the exchanged Ca is very active for the steam gasification [2,3,7]. No exchange reactions would take place significantly in the present work, however, since there are almost no oxygen functional groups as exchangeable sites in petroleum coke, as is expected by very low content of oxygen (Table 1). It should therefore be noted that $\text{Ca}(\text{OH})_2$ loaded on the carbon by simple kneading shows the high catalytic activity for the gasification.

The specific rate of carbon, defined as the gasification rate per unit weight of remaining carbon, is plotted as a function of conversion in Figure 2. The rate of the $\text{Ca}(\text{OH})_2$ -loaded coke at 800°C was independent of the conversion, and it was comparable to the rate at 1000°C without catalyst. This observation means that the use of $\text{Ca}(\text{OH})_2$ can lower the temperature by 200°C. The rate of the Ca-catalyzed gasification at 850 or 900°C changed as fixed carbon conversion increased, and seemed to have minimum at the conversion of around 50 wt%. Since such the change would be determined by the balance between catalyst agglomeration and enrichment due to the consumption of carbon [8], the decreased rate observed in the conversion range of less than 50 wt% suggests that the agglomeration of Ca catalyst may be dominant at the initial stage of reaction. At 900°C the initial rate of the catalyzed gasification was 90 times as large as that of the uncatalyzed one.

As is seen in Figure 2, CaCO_3 also promoted the gasification remarkably. The initial rate at 850°C was lower than that with $\text{Ca}(\text{OH})_2$, but it increased gradually with increasing conversion, and both rates were almost the same at the latter part of reaction. The use of CaCO_3 as alternative to $\text{Ca}(\text{OH})_2$ is interesting from a practical point of view, since limestone and seashell wastes as received can be used as catalyst sources.

Catalyst State and Reactive Sites

Strong, sharp diffraction lines of $\text{Ca}(\text{OH})_2$ were observed on the $\text{Ca}(\text{OH})_2$ -loaded coke. When the coke was devolatilized in pure N_2 , these lines disappeared and CaO peaks with very weak intensities appeared. These observations show that $\text{Ca}(\text{OH})_2$ loaded is transformed mostly to non-crystalline species, which suggests catalyst redistribution on devolatilization, possibly the formation of finely dispersed Ca species. The surface of petroleum coke might be mildly oxidized in the kneading process, and the preoxidation and/or mechanochemical effects during kneading, if any, might affect the dispersion of Ca catalyst.

Figure 3 shows the XRD patterns after gasification of petroleum coke with and without $\text{Ca}(\text{OH})_2$ to 50 wt% conversion. $\text{Ca}(\text{OH})_2$ was transformed mainly to CaCO_3 and partly to CaS during gasification. Since CaO was stable in the devolatilization step preceding carbon gasification, as mentioned above, CaCO_3 was formed by the reaction of CaO with CO_2 . The presence of CaS may mean the catalyst deactivation by the sulfur evolved, which may be one reason for the decrease in specific rate with conversion at the initial stage of reaction (Figure 2). Figure 3 also revealed lower diffraction intensities of C(002) lines than those from the corresponding original carbon. Higher d_{002} and lower L_C were observed in the Ca-bearing sample. These observations point out the formation of non-crystalline carbon in the presence of the catalyst.

When the XPS spectra of these gasified samples were measured, the C 1s peak of the Ca-bearing carbon was broad compared with the

original carbon, and the intensities of the spectra at 286-288 eV, attributable to ether and carbonyl bonds, were higher in the presence of the catalyst. Further, the atomic ratio of O/C, determined by the O and C 1s spectra, with Ca was about 5 times as that without Ca. It is evident from the XPS observations that surface oxygen complexes are formed on the carbon to a larger extent during the Ca-catalyzed gasification.

In order to characterize surface oxygen complexes, the TPD runs of gasified samples were carried out, and the results are summarized in Table 2. No significant amount of CO₂ was detectable without Ca catalyst, and CO alone was released with the largest rate at around 950°C, where the CO₂ gasification of the original coke proceeded at an appreciable reaction rate.

On the other hand, CO₂ desorbed in the presence of Ca catalyst. The desorption started at about 550°C, showed a maximal rate at 700°C, and completed at around 750°C. Since the catalyst was present in the form of CaCO₃ after gasification (Figure 3), it is no doubt that CO₂ desorption comes mainly from the decomposition of CaCO₃. However, the peak temperature of CO₂ desorption was much lower than the decomposition temperature of CaCO₃ bulk, and the TPD pattern was broad. Further, as is seen in Table 2, CO desorption occurred significantly at 700°C where CO₂ desorbed at the largest rate. These observations point out strong interactions between CaCO₃ and carbon surface. The CO evolved at 700°C may originate partly from the formation of CaCO₃-C intermediate and subsequent CO desorption [9,10]. The promotion of CaCO₃ decomposition by carbon has been confirmed by the high temperature XRD technique [2]. The total amount of CO₂ released was larger than Ca loading onto petroleum coke, which suggests that surface complexes such as lactone and acid anhydride formed during the Ca-catalyzed gasification may be decomposed into CO₂ [11,12].

Most of CO desorbed in the wide temperature range of 750-1000°C, where the calcium showed high catalytic activity. The total amount of CO released with Ca catalyst was two times as that without Ca (Table 2). Consequently, the presence of the catalyst lead to about four-fold oxygen uptake on carbon. This is in good agreement with the oxygen increase determined by XPS measurements. Since the sample after gasification of the CaCO₃-loaded coke showed almost the same TPD profiles as in the case of Ca(OH)₂, CaCO₃ also enhanced the number of reactive sites. It is probable that the increased sites are responsible for large reactivity of petroleum coke in the presence of Ca(OH)₂ and CaCO₃.

4. CONCLUSION

Ca(OH)₂ or CaCO₃ showed high catalytic activity for the CO₂ gasification of petroleum coke at 800-900°C when loaded by simple kneading. The calcium promoted the formation of surface oxygen complexes on the carbon during gasification.

ACKNOWLEDGMENT

This work has partly been carried out as a research project of the Japan Petroleum Institute commissioned by the Petroleum Energy Center with the subsidy of the Ministry of International Trade and Industry, Japan. The authors gratefully acknowledge Ayumi Shoji and Yasuhiro Ohshima for their assistance in carrying out experiments.

REFERENCES

- 1) Dymond, R.E. *Hydrocarbon Processing* 1991, September, 162-C.
- 2) Ohtsuka, Y.; Tomita, A. *Fuel* 1986, 65, 1653.
- 3) Ohtsuka, Y.; Asami, K. *Energy Fuels* 1995, in press.
- 4) Ohtsuka, Y.; Asami, K. *Energy Fuels* in press.
- 5) Martin, R.R.; Macphee, J.A.; Kyotani, T.; Hayashi, S.; Tomita, A. *Carbon* 29, 475.
- 6) Kyotani, T.; Hayashi, S.; Tomita, A. *Energy Fuels* 1991, 5, 683.
- 7) Nabatame, T.; Ohtsuka, Y.; Takarada, T.; Tomita, A. *J. Fuel Soc. Japan* 1986, 65, 53.
- 8) Asami, K.; Ohtsuka, Y. *Ind. Eng. Chem. Research*, 1993, 32, 1631.
- 9) Cazorla-Amorós, D.; Linares-Solano, A.; Salinas-Martinez de Lecea, C.; Joly, J.P. *Carbon* 1991, 29, 361.
- 10) Cazorla-Amorós, D.; Linares-Solano, A.; Salinas-Martinez de Lecea, C.; Kyotani, T.; Yamashita, H.; Tomita, A. *Carbon* 1992, 30, 995.
- 11) Koenig, P.C.; Squires, R.G.; Laurendeau, N.M. *Carbon* 1985, 23, 531.
- 12) Zhuang, Q.; Kyotani, T.; Tomita, A. *Energy Fuels* 1995, 9, 630.

Table 1 Analysis of petroleum coke used

Ash (wt%, dry)	V.M.	C	H	N	S	O	d_{002} (nm)	L_c
				(wt%, daf)				
0.3	11.2	89.4	4.0	2.5	2.1	2.0	0.348	2.5

Table 2 Desorption of CO₂ and CO from the samples gasified at 850°C

Catalyst	Peak temperature (°C)		Total amount released (mmol/g)	
	CO ₂	CO	CO ₂	CO
None	n.d. ^a	950	n.d. ^a	7
Ca(OH) ₂	≈700	700 ^b , 900-1000	8	14

^aNot detectable. ^bShoulder peak.

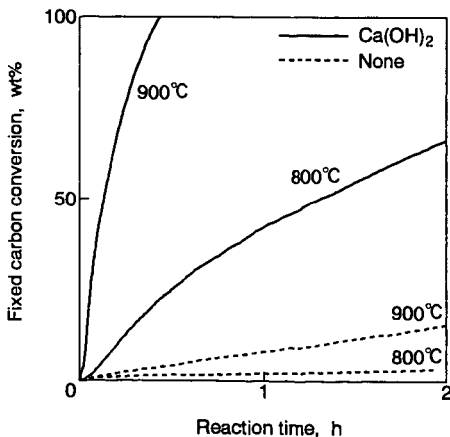


Figure 1. Profiles for the gasification of petroleum coke with CO₂.

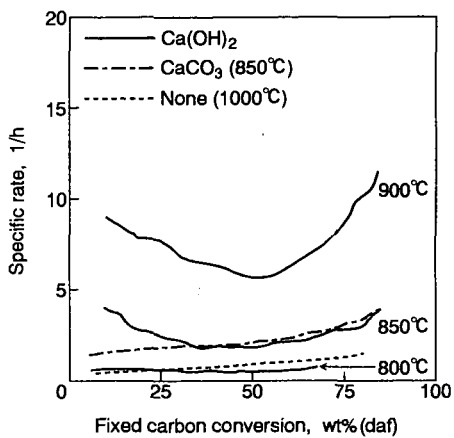


Figure 2. Relationship between specific rate and fixed carbon conversion.

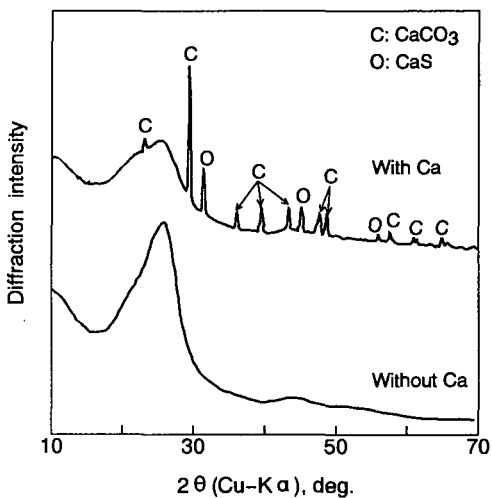


Figure 3. X-ray diffraction patterns of gasified samples with and without Ca catalyst.

LOW TEMPERATURE CATALYTIC COMBUSTION OF CARBON BY ALKALI METAL SALT/PEROVSKITE TYPE OXIDE MIXTURE

Tatsuro Miyazaki, Masahiro Inoue, and Isao Mochida*
Material&Component Research Laboratory, Kyushu Matsusita Electric
Co.,Ltd. Minosima, Hakata-ku, Fukuoka 812 Japan,
*Institute of Advanced Material Study, Kyushu University
Kasugakoen, Kasuga-shi, Fukuoka 816 Japan

Key words : Catalytic combustion, Alkali salt, Perovskite type oxide

Introduction

Alkali metal salts have been reported the best catalysts for the carbon combustion.^{1,2)} However, their active species have been recognized to vaporize out from the combustion zone.³⁾ Some transition metal oxides has been reported active to catalyze the combustion and gasification of carbon.^{4,5)} However, their intimate contact with the carbon substrate should be assured for the catalysis. Enhancement of catalytic activity has been examined by increasing dispersions and controlling composition.^{6,7)} However, maintenance of contact with the separate carbon grains to increase the conversion has not been attempted.

In the present study, catalytic activity of alkali metal salts supported on γ - Al_2O_3 and perovskite type oxide for the combustion of active carbon was studied, to find a way to realize the repeated contact of alkali metal species with carbon through their sublimation and precipitation over the surface of the perovskite type oxide. Influence of anions of salts, mixing procedures of the catalyst, support and carbon as well as the reaction temperature, were examined. The elution of active species was also estimated to observe the combustion of carbon placed at the down-stream of the catalyst bed.

Experimental

Activated carbon (AC) (Nacalai tesque inc.; surface area 370 m^2/g) was used, after washing with hydrochloric acid aq. to remove ash and heat treated at 973K for 8h in nitrogen. Ultimate analysis showed that resulting AC carried small amount of mineral matter (0.01wt%), being free from any detectable hydrogen, oxygen, nitrogen or sulphur. Supported catalysts were prepared by the impregnation. A prescribed amount of potassium metal salts (K_2CO_3 , KCl, K_2SO_4) were dissolved in deionized water.

The AC, Al_2O_3 (Nikkei Kinzoku Co. ,Ltd.), perovskite type oxide used as carrier material was dispersed in the solution and then heated to dryness at 363K for 12h. The catalyst loading was adjusted to 1.3×10^{-3} atom alkali per total amount of carrier and reactant (AC) (g).

Perovskite type oxide was prepared from the mixture of component metal nitrates or acetates, through vigorous mixing in water, freeze-dry and calcined at 1123K for 5h. X-ray diffraction analyses showed perovskite type structure of mixed oxide. Examined composition of perovskite was $\text{La}_{0.8}\text{Sr}_{0.2}\text{Cr}_{0.5}\text{Mn}_{0.45}\text{Pt}_{0.05}\text{O}_3$ (LSCMP).

A continuous flow reactor apparatus was operated under atmospheric pressure. In order to prevent local accumulation of heat, an initial ratio of AC to catalyst was 0.1. The mixture of AC and catalyst was dispersed on a ceramic foam (Brigestone Co. Ltd.). A thermocouple was located at the end of catalyst bed. N_2 was flowed during the heating to the reaction temperatures and the oxidant gas (N_2 containing 4% O_2) was introduced for the combustion. The gaseous products were analyzed by IR-spectrometer (Simadzu Co. ,Ltd.). The amount of AC consumed was determined by the product gas analysis.

Results

Catalytic activity of supported potassium carbonate catalysts

Figure 1 shows AC combustion catalyzed by supported K_2CO_3 as function of time at 723K. The activity of supported K_2CO_3 catalysts used in this study increased in the order; $\text{K}_2\text{CO}_3/\gamma\text{-Al}_2\text{O}_3 < \text{K}_2\text{CO}_3/\text{Pt-}\gamma\text{-Al}_2\text{O}_3 < \text{K}_2\text{CO}_3/\text{AC} < \text{K}_2\text{CO}_3/\gamma\text{-Al}_2\text{O}_3$ blended with LSCMP $< \text{K}_2\text{CO}_3/\text{LSCMP}$. The activity of supported K_2CO_3 catalysts was significantly influenced by the supports;

particularly, K_2CO_3 supported on LSCMP catalyst showed the largest activity among the catalysts tested. Because the activity of LSCMP was not so high, K_2CO_3 supported LSCMP performed the catalysis of very rapid combustion within 500 sec, increasing the conversion upto 100%. $K_2CO_3/\gamma-Al_2O_3$ physically blended with LSCMP showed high activity than $K_2CO_3/\gamma-Al_2O_3$, giving c.a.100% conversion within 2000 sec. K_2CO_3 supported on AC, Pt- $\gamma-Al_2O_3$, and $\gamma-Al_2O_3$ showed rapid combustion at low conversion level, however the conversion was saturated at 60%.

Catalytic activity of supported potassium salts

Figure 2 summarizes the activity of potassium salts supported on $\gamma-Al_2O_3$ blended with or without LSCMP at 723K. First of all, $KCl/\gamma-Al_2O_3$ showed the largest activity among the salts supported on $\gamma-Al_2O_3$, obtaining nearly 100% combustion by 3000 sec. The $K_2SO_4/\gamma-Al_2O_3$ exhibited the lowest activity.

The effectiveness of the blended catalysts with LSCMP depended very much on the type of potassium salts. The blended catalysts of $K_2CO_3/\gamma-Al_2O_3$ with LSCMP exhibited the strongest synergistic effect to show the largest activity among the potassium salts tested. KCl blended with LSCMP exhibited lower activity than $KCl/\gamma-Al_2O_3$.

Analysis for disappearance of potassium on catalysts

In order to estimate potassium amount on carriers after the combustion reaction, the catalytic combustion was repeated three times, using the same catalyst. $K_2CO_3/\gamma-Al_2O_3$ and $K_2CO_3/LSCMP$ were mixed with carbon respectively, and then were heated to 873K under air flow (700 ml/min.). The potassium element remaining on these catalysts was extracted with HCl aq., and analyzed by capillary zone electrophoresis(SZE). Table 1 showed the diminution ratio of the potassium amount before and after reactions. $K_2CO_3/\gamma-Al_2O_3$ lost significant amount of K after the reaction, but less loss of potassium was detected on $K_2CO_3/LSCMP$.

And then to estimate outflow of potassium element from catalyst bed to down-stream, the combustion reactions were executed at 723K. AC was mixed with $K_2CO_3/LSCMP$ and $K_2CO_3/\gamma-Al_2O_3$ respectively in the same way as mentioned above. Then AC was placed at the down-stream of the catalyst bed.

The results are shown in Figure 3. The activities of $K_2CO_3/LSCMP$ and $K_2CO_3/\gamma-Al_2O_3$ are in it for references. The conversion(X) in this figure is defined as

$$X=(W_o-W-W_b)/(W_o-W_b)$$

where W_o is the initial amount of AC, which was mixed with catalyst, W is the combustion amount of AC at reaction time, W_b is the combustion amount of AC without catalyst at reaction time.

The combustion profiles over $K_2CO_3/LSCMP$ were similar regardless of the down flow carbon. In contrast, $K_2CO_3/\gamma-Al_2O_3$ increased the conversion of AC when the AC free from catalyst was placed at the down stream. Some catalysts may be transferred bed carrying the catalyst to the down stream.

Influence of reaction temperature

Figure 5 shows the catalytic activity of $K_2CO_3/\gamma-Al_2O_3$, $K_2CO_3/LSCMP$, and blended $K_2CO_3/\gamma-Al_2O_3$ with LSCMP at 623~723K.

$K_2CO_3/LSCMP$ exhibited the highest activity of these three catalysts at this temperature range. Although the activity of $K_2CO_3/\gamma-Al_2O_3$ blended with LSCMP was same to that of $K_2CO_3/\gamma-Al_2O_3$ at 423 K, the blended catalyst exhibited the higher activity at higher temperatures.

Discussion

Potassium salts have been reported to catalyze the combustion of the carbon through their reduction into metal to activate oxygen⁸). The alkali metal can sublime to be mobile over the carbon substrates, maintaining the intimate contact for the catalytic activity. On the other hand, sublimed metal may flow out from the carbon bed, no catalytic activity being maintained. Thus, the sublimation and precipitation of the metal should be

balanced in the carbon bed for the maintenance of the catalytic activity.

LSCMP appears a unique support to perform such sublimation and precipitation for catalytic activity. Another role of the support is to influence the decomposition of potassium salts into active species, LSCMP appears to have such a role. Questions why LSCMP performs such roles are not answered in this paper. Further research is attempted.

KCl/ γ -Al₂O₃ exhibited a unique activity to show stable activity, achieving nearly 100% conversion. Active species for KCl/ γ -Al₂O₃ is now studied.

References

- 1) Walker, Jr., P.L., Shelef, M., Anderson, R.A., "Chemistry and physics of carbon", ed. by walker, Jr., P.L., vol.4, marcel Dekker, New York 1986, 287.
- 2) Mckee, D.W., Chatterji, D., Carbon, 1975, 13, 381.
- 3) Marsh, H., Mochida, I., ECSE Report, 1978.
- 4) Backer, R.T., Chludzinski, Jr., Carbon, 1981, 19, 75.
- 5) Carrazza, J., Tysoe, W.T., Heinemann, H., Somorjai, G.A., J.Catal., 1985, 96, 234.
- 6) Mochida, I., Gao, Y.-Z., Fujitsu, H., Sekiyu Gakkai, 1991, 34, 178.
- 7) Mckee, D.W., "Chemistry and physics of carbon", ed. by walker, Jr., P.L., vol.16, marce Dekker, New York 1981, 1.
- 8) Frinks, I.L.C., van Wechem, H.M.H., Stuiiver, J.C.M., Bouwman, R., Fuel, 1981, 60, 463.

Table1 Potassium diminution ratio of K before and after reaction by CZE

Catalyst	Diminution ratio
K ₂ CO ₃ / γ -Al ₂ O ₃	55.5%
K ₂ CO ₃ /LSCMP	8.0%

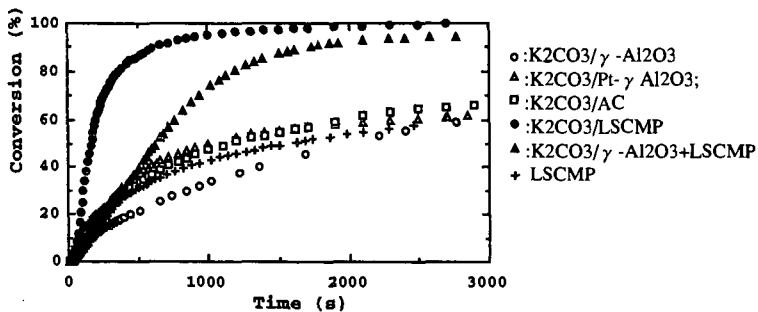


Fig.1 Conversion of carbon catalyzed by supported potassium carbonate

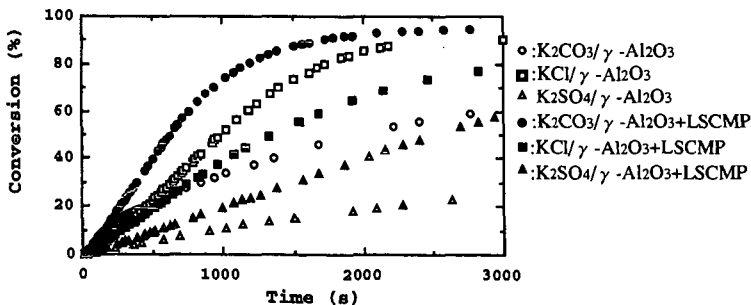


Fig.2 The activity of potassium salts supported on γ -Al₂O₃ blended with or without LSCMP

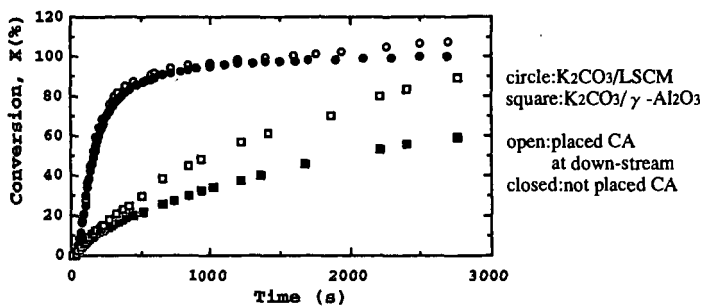


Fig.3 The conversion of carbon placed at down-stream of carbon/supported potassium carbonate bed

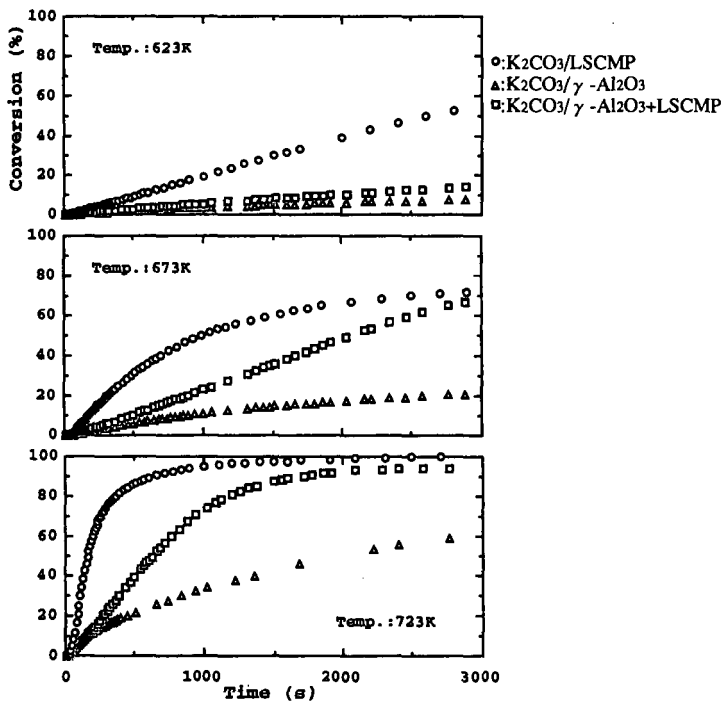


Fig.4 The activity of supported K_2CO_3 catalysts at some temperatures

DRIFT ANALYSIS OF SURFACE OXYGEN COMPLEXES ON SOOT FORMED BY METAL OXIDES

G. Mul, F. Kapteijn and J.A. Moulijn

Delft University of Technology, Section Industrial Catalysis,
Julianalaan 136, 2628 BL Delft, The Netherlands.

Keywords : DRIFT, Surface Oxygen Complexes, Metal Oxides.

INTRODUCTION

At the Delft University of Technology a project concerning the catalytic removal of soot from diesel exhaust gases is being carried out. We are interested in a catalyst for the oxidation of soot particulates because: (i) diesel engines can no longer meet the requirements of the particulate (soot) emission standards, and (ii) collection of soot in a monolithic filter and simultaneous oxidation at diesel exhaust gas temperatures (600 K) is considered to be the best option to abate the emission of soot.

The mechanism of catalytic oxidation reactions of carbonaceous materials has been the subject of many researchers over the last decades. Although it has been generally expected that Surface Oxygen Complexes (S.O.C.) play an essential role in these reactions, their chemical nature, and interaction with catalysts and the oxidant (CO_2 , H_2O or O_2) have hardly been reported. A powerful tool in analyzing carbonaceous materials is Fourier Transformed Infrared spectroscopy and in particular Diffuse Reflectance Infrared Fourier Transformed (DRIFT) spectroscopy. Several research groups have analyzed coal of several ranks using this technique *e.g.* (1-3). Also *in situ* studies regarding the oxidation of coal have been performed (4-6), as well as DRIFT studies on oxidized soot (7,8) and PF chars (9). Very few researchers have used DRIFT spectroscopy to analyze the catalytic oxidation of carbon or soot. Cerfontain has studied the alkali carbonate catalyzed carbon oxidation by CO_2 by means of FT-IR (10), but carbon oxidation involving O_2 and (transition) metal oxides have only been reported by us (11). It has been shown that during burn-off certain metal oxides enhance the amount of S.O.C. on the soot surface, while others do not. This observation has been explained by two different reaction mechanisms: (i) a redox mechanism and (ii) a spill-over mechanism (11). However, these results were obtained with catalyst/soot mixtures with a high catalyst to soot ratio (1:1, *i.e.* 50 wt%). In this paper DRIFT analyses of partially converted soot by impregnated Fe-, Co-, Cr-, K-, and Ca- oxides (10 wt%) are presented, which validates a comparison of these analyses with literature data on catalyzed carbon and coal gasification.

EXPERIMENTAL

Printex-U (a model soot, purchased from Degussa) was used to perform the oxidation studies. This soot has a BET surface area of $96.0 \text{ m}^2 \text{ g}^{-1}$ and contains approximately 5 wt% of adsorbed hydrocarbons and only 0.2-0.4 wt% sulfur (12).

Analytical grades of the (transition) metal nitrates were used to impregnate the soot. An amount of the nitrate, corresponding with 10 wt% of the most stable oxide (Fe_2O_3 , Co_3O_4 , Cr_2O_3 , K_2O , and CaO) was dissolved in 200 ml ethanol, followed by addition of 200 mg soot to the solution. The ethanol was removed at 325 K under reduced pressure in a rotating evaporator. The black powder could be recovered by scratching it from the glass wall of the flask with a spatula.

Partial conversion of the soot was accomplished in a so-called six-flow reactor. A six-flow experiment was carried out by packing five quartz reactors (one reactor was used as a blank) with approximately 25 mg of the impregnated soot/metal nitrate mixture, sandwiched between two layers of SiC. A controlled flow of 150 ml/min. 10 vol% O_2 in Ar was led through the reactors. A non dispersive infrared detector (Hartmann & Braun Uras 10 E) was used to measure CO, CO_2 and NO concentrations. These concentrations were measured alternately every 90 seconds in each reactor. A multiposition valve (Valco) selected the reactor for analysis. The partial conversions were obtained isothermally @ 575 K (K, Co) and @ 585 K (Ca, Fe, Cr). The final temperature was reached with a ramp of 5 K/min. The amount of soot converted was determined by integrating the CO and CO_2 concentrations with time. After reaction SiC was separated from the soot sample before analysis.

DRIFT spectra were recorded on a Nicolet Magna 550 spectrometer equipped with a DTGS detector and a Spectratech DRIFT accessory. KBr was used as a diluent. Spectra are displayed in 8 cm^{-1} resolution in absorbance reflectance mode against a (*non*-converted) soot in KBr background.

RESULTS & DISCUSSION

Transition metal nitrates

A typical result of the analysis of one reactor in a sixflow measurement is shown in figure 1. The variations in the CO, CO₂ and NO concentrations as a function of time are given for the Fe(NO₃)₃/soot sample. Decomposition of Fe(NO₃)₃ into N₂O, NO and NO₂ (the concentrations of N₂O and NO₂ were not determined) occurs at approximately 450 K. As NO₂ is a strong oxidant, reaction of NO₂ with soot results in NO, CO and CO₂ formation (13). The reaction of NO₂ with soot is reflected by high NO, CO and CO₂ concentrations in the first 6 ks of the reaction, when the temperature is still increasing with time. After the temperature has become constant @ 585 K (the temperature was isotherm between the verticle dashed lines), the CO and CO₂ concentrations decrease exponentially with time. A similar trend was obtained for the Co(NO₃)₂/soot sample @ 575 K (not shown). By integration of the CO and CO₂ concentrations, soot conversion was calculated to be 20% for the Fe(NO₃)₃/soot, and 50% for the Co(NO₃)₂/soot mixture respectively.

Variations in the CO, CO₂ and NO concentrations @ 585 K for the impregnated Cr(NO₃)₃/soot mixture are shown in figure 2. Similar to the Fe(NO₃)₃ measurement, a rapid decomposition of the nitrate into (presumably) Cr₂O₃ can be observed at 400 K, accompanied by high NO, CO and CO₂ concentrations. In the isothermal part, the development of the CO and CO₂ concentrations is quite different from the Fe(NO₃)₃ sample. Instead of a decay, a slow increase in the CO and CO₂ concentrations can be observed. A similar result has been obtained for a mechanical mixture of Cr₂O₃ and soot (14). The soot conversion was calculated to be 50%. Another six-flow experiment was performed upto a conversion level of 20%.

The DRIFT spectra of the partially converted Fe(NO₃)₃/soot (20% (A)), Co(NO₃)₂/soot (50% (B)) and Cr(NO₃)₃/soot (20% (C) and 50% (D)) samples are shown in figure 3. Infrared absorptions which are typical for compounds containing (hydrated) nitrate groups (1560-1540, 1020-1070, 800 and 760 cm⁻¹) (15) are not present in the spectra. The absorptions located @ 665 and 578 cm⁻¹ (spectrum B) can be ascribed to the spinel vibrations of Co₃O₄. The broad absorption band @ 549 cm⁻¹ is ascribed to Cr₂O₃ (spectra C and D). Hence, confirming the six-flow analysis, the transition metal nitrates were completely converted into their oxides. Generally three types of Surface Oxygen Complexes (S.O.C.) can be identified with DRIFT on soot (or carbon) surfaces: (i) ethers (1250-1275 cm⁻¹), (ii) quinones (1600-1620 cm⁻¹), and (iii) lactones (1730-1740 cm⁻¹) (9). On the surface of the partially converted soot by Cr(NO₃)₃ (Cr₂O₃) large quantities of these S.O.C. were formed. The spectra of the Fe₂O₃ and Co₃O₄ samples show approximately the same amount of S.O.C. as were formed *non*-catalytically on soot under similar conditions. These results are in agreement with the results obtained for mechanical mixtures of Cr₂O₃, Fe₂O₃ and Co₃O₄ with soot (11).

Potassium nitrate

The activity in the soot oxidation of KNO₃ is shown in figure 4. KNO₃ decomposition is not as fast as the decomposition of the transition metal nitrates. Moreover, the maxima in the CO and CO₂ concentrations do not coincide with the maximum in the NO concentration. Apparently the peculiar "peaks" in the CO and CO₂ concentrations are not entirely explained by the NO₂/soot reaction. After the "peaks", the CO and CO₂ concentrations decay linearly in time. The calculated conversion was 75%.

DRIFT spectra of KNO₃/soot samples at conversion levels of 0% (A), 50% (B), 75% (C), and >90% (D) are shown in figure 5. Spectrum A corresponds quite well with the spectrum of pure KNO₃ (the 1383 cm⁻¹ vibration can be assigned to a nitrate vibration (15)). After 50% soot conversion, the 1383 cm⁻¹ vibration is no longer present. Hence, the nitrate has decomposed. Although ether-like species are not so clearly present (@ 1250-1300 cm⁻¹), the absorptions located @ 1721 cm⁻¹ and 1595 cm⁻¹ indicate that (a) potassium oxide catalyzes the formation of S.O.C. These absorptions are increasing with the conversion level, and shifted to somewhat lower wavenumbers, compared to the spectra shown in figure 3. This might indicate that a potassium oxide is in the vicinity of the S.O.C.

Carbonate formation is witnessed by broad absorption bands @ 1456 cm⁻¹ and 871 cm⁻¹ (15,22), which are clearly present in the spectrum of the sample converted to >90% (spectrum D). Other absorption bands, @ 1118 cm⁻¹ and 620 cm⁻¹, are increasing with conversion. Also impregnated Rb and Cs oxides cause the formation of these absorptions during burn off. We are still speculating on the nature of the (potassium) compound responsible for these absorptions. The assignment of these bands to potassium sulfate, which has vibrations in the 1100-1200 cm⁻¹ region, is not likely, because the amount of sulfur initially present in the soot (Printex-U) is low and the sulfate-ion has a more complex IR pattern than shown in figure 5 (15). The 1118 cm⁻¹ band has been observed by other authors in the K₂CO₃ catalyzed carbon gasification with CO₂ (10) and steam (16). Cerfontain (10) and Freriks (16) did not detect the 620 cm⁻¹ band, because they did not record their spectra below 1000 cm⁻¹. In our opinion this absorption is related to the 1118 cm⁻¹ one. The 1118 cm⁻¹ band has been assigned to a potassium phenolate (10). However,

the carbon-oxygen vibration of potassium phenolate (or phenoxide) occurs at much higher wavenumbers (around 1300 cm^{-1} (17), verified by ourselves). The mass difference of a phenoxide and a poly-aromatoxide ion can only partly account for a red shift of 150 cm^{-1} . Unless the frequency of C-OK vibrations is strongly influenced by the vicinity of other C-OK groups (e.g. in the compound proposed by Freriks (16)) or other oxygenated species, the assignment of the 1118 cm^{-1} vibration to phenolate species is not very likely. A second proposition for the assignment of the 1118 cm^{-1} band is based on the following: the structure of alkali metal catalysts under gasification conditions is thought to be a potassium oxide (K_2O) cluster attached to the carbon surface (18). It has been shown that CO_2 adsorption on the potassium oxide cluster is very strong (18,19). Therefore, the 1118 and 620 cm^{-1} absorptions might be the result of CO_2 (formed during soot oxidation) strongly interacting with a potassium oxide cluster. Interestingly, similar absorptions have been reported in studies on CO_2 adsorption on Cu_2O (20) and CuO (21).

Calcium nitrate

Decomposition of calcium nitrate is less rapid than decomposition of the transition metal nitrates (figure 6). Although some NO (and CO and CO_2) production takes place during the temperature ramp, a considerable amount of nitrate decomposes in the isothermal stage. For some reason, the decomposition rate increases with time. The NO , CO and CO_2 concentrations run parallel, indicating that the primary product of nitrate decomposition is NO_2 , which subsequently oxidizes the soot, resulting in the observed products. After complete decomposition of $\text{Ca}(\text{NO}_3)_2$, a second increase in reaction rate can be observed. The measurement shown in figure 6 resulted in 50% soot conversion.

DRIFT spectra of $\text{Ca}(\text{NO}_3)_2 \cdot 4\text{H}_2\text{O}$ /soot samples (0% (A), 20% (B), 50% (C) and >90% (D) soot conversion) are shown in figure 7. After preparation several absorptions occur in the $500\text{--}2000\text{ cm}^{-1}$ region of the spectrum, due to nitrate vibrations (@ 1384 , 1046 and 838 cm^{-1}). The absorption band @ 1635 cm^{-1} can be ascribed to the O-H bending mode of water of crystallization in $\text{Ca}(\text{NO}_3)_2 \cdot 4\text{H}_2\text{O}$ (23). The broad band located @ 1433 cm^{-1} is also present in the DRIFT spectrum of pure $\text{Ca}(\text{NO}_3)_2 \cdot 4\text{H}_2\text{O}$. After 20% soot conversion @ 575 K , the nitrate vibrations are still present, which is in agreement with six-flow data. The 1433 cm^{-1} band has broadened and a new vibration, located at approximately 1579 cm^{-1} , can be observed. At higher conversions (spectra C and D) the vibrations due to the nitrate group have disappeared and are replaced by the vibrations ascribed to the carbonate group (CaCO_3 (14,23,24)) @ 712 cm^{-1} , 875 cm^{-1} , centred @ 1436 cm^{-1} , and 1795 cm^{-1} . The 1579 cm^{-1} band has shifted somewhat to 1587 cm^{-1} . Also a broad absorption band starts to develop @ 1142 cm^{-1} . This band is clearly visible in the spectrum of the >90% soot conversion. In the latter spectrum, the 1587 cm^{-1} vibration is no longer present.

Absorptions due to regular lactone, quinone and ether like complexes are hardly visible. However, the 1587 cm^{-1} absorption is related to the presence of soot, because this absorption frequency is not visible after 90% soot conversion. Probably this band is due to quinone species. The shift of approximately 20 cm^{-1} might be caused by some kind of interaction with a Ca-ion. The broad 1142 cm^{-1} absorption might be related to the 1118 cm^{-1} absorption band observed in the KNO_3 /soot spectra.

Mechanistic considerations

The investigated metal nitrate precursors show an increasing reactivity in the order $\text{K} > \text{Co} > \text{Cr} > \text{Fe} = \text{Ca}$. The activities of the impregnated samples are higher than the activities found for the mechanical mixtures of the metal oxides and soot (11). Especially the activity of the impregnated chromium nitrate is much higher than the activity of bulk Cr_2O_3 . The differences in reactivity might be explained by a better dispersion of the oxides formed after decomposition of the impregnated nitrates. X-Ray Diffraction and Transmission Electron Microscopy studies are currently being performed to determine the particle size of the various impregnated nitrates and oxides.

The DRIFT spectra shown in this paper indicate that the formation of S.O.C. is dependent on the catalyst used. In the presence of K, Ca and Cr catalysts, S.O.C. are catalytically formed. The differences in CO and CO_2 concentration profiles shown in figures 1,2,4 and 6, are very likely related to this formation of S.O.C. Catalysts which do not enhance the formation of S.O.C., show an exponential decay, while catalysts which increase the amount of S.O.C. show a less pronounced activity loss (K), or even an activity increase (Cr, Ca). The differences in reactivity profiles is discussed in more detail elsewhere (14).

A redox cycle is often proposed as the most likely mechanism by which metal oxides operate in the oxidation of carbon (e.g. (25,26)). Other authors mention spill-over of oxygen to explain catalytic carbon oxidation. Baker et al. (27) argued, explaining their Controlled Atmosphere Electron Microscopy (CAEM) studies, that Cr_2O_3 was able to dissociate molecular oxygen and to transfer the activated oxygen to the carbon surface. Eventually, reaction occurred

at the graphite edges. This might indicate that the enhanced formation of S.O.C. is related with oxygen spill-over.

Oxygen spill-over has never been proposed for alkali metal carbon gasification reactions (28-31). However, the mechanism proposed by Meijer and Moulijn (21) involves the transfer of oxygen from a K-oxide cluster to an active carbon site, which could be interpreted as spill-over. Reaction of this transferred oxygen results in the formation of S.O.C. Kapteijn *et al.* (32), discussing a transient isotopic CO₂ gasification study, describe several kinds of S.O.C., which they indicate as C(O)C(O) (lactone) and C₂(O) (semi-quinone). The DRIFT spectra presented in this paper show, in agreement with the literature data, that upon carbon (soot) oxidation several S.O.C. are formed, probably in the vicinity of a potassium oxide cluster.

The spill-over effect was also mentioned by Kyotani and Tomita *et al.* in relation with Ca catalyzed graphite oxidation (33-36). Although Martin and Kyotani *et al.*, using SIMS and TPD, did not reveal the nature of the S.O.C. formed after Ca catalyzed oxidation (35), they indicated that the distribution of the S.O.C. corresponded to the distribution of the Ca catalyst. This is in agreement with the fact that we observe a shift of the 1605 cm⁻¹ quinone band to lower wavenumbers, which could be induced by the presence of Ca ions. The fact that we were unable to detect lactone species (or C(O.O) (33)), formed by reaction of a C(O) complexes with an activated oxygen atom, might be due to a very fast, Ca induced, desorption of those complexes (as CO₂). The nature and role of the species absorbing @1142 cm⁻¹, is not clear at this moment.

Evaluating the presented DRIFT spectra and literature mentioned, we believe that the catalytic formation of S.O.C. must be related to some kind of oxygen spill-over mechanism. The intensity and frequency of the absorptions of the S.O.C. might be indicative for the stability and the vicinity of a metal oxide. Catalysts which do not enhance the amount of S.O.C. are thought to be active according to a redox-mechanism (11,14).

CONCLUSIONS

- The transition metal nitrates decompose in air at approximately 450 K. DRIFT analysis revealed that metal oxides are formed upon decomposition.
- The results of the DRIFT analyses of impregnated samples are in agreement with the results presented earlier (11) for mechanically mixed soot/transition metal oxide mixtures. Cr₂O₃ causes an enhancement of the amount of S.O.C. (compared to non-catalytic oxidation), whereas Co₃O₄ and Fe₂O₃ do not.
- Alkali metal nitrates are less easily converted into their corresponding oxides. After decomposition an alkalimetal oxide attached to the carbon surface is being formed. The exact nature of this compound remains to be elucidated.
- Alkali metal oxides enhance the amount of S.O.C. The IR absorption band of the quinone species is shifted from 1605 cm⁻¹ to 1585 cm⁻¹. Also the lactone vibration (1735 cm⁻¹) is shifted to lower wavenumbers, indicating the vicinity of a potassium ion.
- Ca(NO₃)₂ is the most stable of the nitrates investigated, and decomposes into CaCO₃ upon soot oxidation. Also an "alkali metal like" complex on the soot surface is eventually being formed. CaCO₃ probably generates quinone species, whereas lactones are not formed.
- The catalytic formation of S.O.C. by Cr, K, and Ca, as shown by the DRIFT spectra presented in this paper, is tentatively explained by "spill-over" of activated oxygen. This is in reasonable agreement with data reported in the literature.

REFERENCES

1. Smyrl, N.R. and Fuller, E.L. *Appl. Spectrosc.* **41**, 1023 (1987).
2. Fuller, E.L. and Smyrl, N.R. *Appl. Spectrosc.* **44**, 451 (1990).
3. Meldrum, B.J. and Rochester, C.H. *J. Chem. Soc. Faraday Trans.* **86**, 1881 (1990).
4. Meldrum, B.J. and Rochester, C.H. *J. Chem. Soc. Faraday Trans.* **86**, 2997 (1990).
5. Rochester, C.H. and Meldrum, B.J. *J. Chem. Soc. Faraday Trans.* **86**, 861 (1990).
6. Meldrum, B.J., Orr, J.C., and Rochester, C.H. *J. Chem. Soc. Chem. Commun.* 1176 (1985).
7. Jassim, J.A., Lu, H.P., Chughtai, A.R., and Smith, D.M. *Appl. Spectrosc.* **40**, 113 (1986).
8. Akhter, M.S., Chughtai, A.R., and Smith, D.M. *Appl. Spectrosc.* **45**, 653 (1991).
9. Zhuang, Q.-L., Kyotani, T., and Tomita, A. *Energy & Fuels* **714** (1994).
10. Cerfontain, M.B., Moulijn, J.A. *Fuel* **62**, 256 (1983).
11. Mul, G., Kapteijn, F., and Moulijn, J.A. *Proc. 22nd Biennial Conf. on Carbon, San Diego* 554 (1995).
12. Neef, J.P.A., "Catalytic oxidation of soot-Potential for reduction of diesel particulate emissions", PhD Thesis, TU Delft, p. 71 (1995).
13. Cooper, B.J. and Thoss, J.E. *SAE Paper 890404*, 171 (1989).
14. Neef, J.P.A., "Catalytic oxidation of soot-Potential for reduction of diesel particulate emissions", PhD Thesis, TU Delft, p. 165 (1995).
15. Ross, S.D. "Inorganic Infrared and Raman Spectra" McGraw-Hill Book Company, London, 1972.

16. Freriks, I.L.C. *Fuel* **60**, 463 (1981).
17. Davies, M. and Jones, R.L. *J. Chem. Soc.* **42**, 121 (1954).
18. Moulijn, J.A. and Kapteijn, F. *Carbon* **33**, 1155 (1995).
19. Meijer, R., van der Linden, B., Kapteijn, F., and Moulijn, J.A. *Fuel* **70**, 205 (1991).
20. Busca, G. J. *Mol. Catal.* **43**, 225 (1987).
21. Davydov, A.A. and Budneva, A.A. *React. Kinet. Catal. Lett.* **25**, 121 (1984).
22. Schutte, C.J.H. and Bujijs, K. *Spectrochim. Acta* **17**, 921 (1961).
23. Nyquist, R.A. and Kagel, R.O. "Infrared Spectra of Inorganic Compounds" Academic Press, New York, 1971.
24. Sterzel, W. and Chorinsky, E. *Spectrochim. Acta* **24A**, 353 (1968).
25. McKee, D.W. *Fuel* **62**, 170 (1983).
26. McKee, D.W. *J. Catal.* **108**, 480 (1987).
27. Baker, R.T.K. and Chludzinski, J.J. *Carbon* **19**, 75 (1981).
28. Yuh, J.Y. and Wolf, E.E. *Fuel* **62**, 252 (1981).
29. Mims, C.A. and Rose, K.D. *J. Am. Chem. Soc.* **104**, 6886 (1982).
30. Silva, I.F. and Lobo, L.S. *Fuel* **65**, 1400 (1986).
31. Meijer, R., Kapteijn, F., and Moulijn, J.A. *Fuel* **73**, 723 (1994).
32. Kapteijn, F., Meijer, R., Moulijn, J.A., and Cazorla-Amoros, D. *Carbon* **32**, 1223 (1994).
33. Kyotani, T., Hayashi, S., and Tomita, A. *Energy and Fuels* **5**, 683 (1991).
34. Kyotani, T., Hayashi, S., Tomita, A., MacPhee, J.A., and Martin, R.R. *Fuel* **71**, 655 (1991).
35. Martin, R.R., MacPhee, J.A., Kyotani, T., Hayashi, S., and Tomita, A. *Carbon* **29**, 475 (1991).
36. Martin, R.R., MacPhee, J.A., Kyotani, T., Hayashi, S., and Tomita, A. *Proc. 20th Biennial Conf. on Carbon, Santa Barbara*, 490 (1991).

ACKNOWLEDGEMENT

The research described in this publication was supported by the Netherlands Foundation for Chemical Research (SON) with financial aid from the Netherlands Organisation for Scientific Research (NWO).

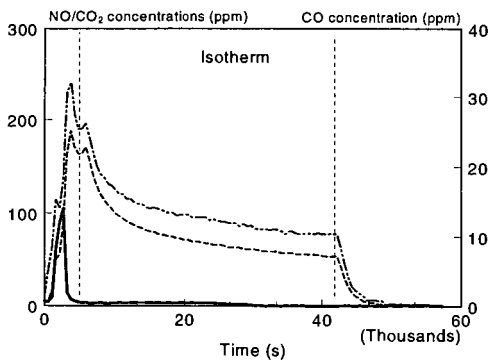


Figure 1. $\text{Fe}(\text{NO}_3)_3$ catalyzed soot oxidation. Development of NO (solid), CO_2 (dash) and CO (alternating dash) concentrations in time.

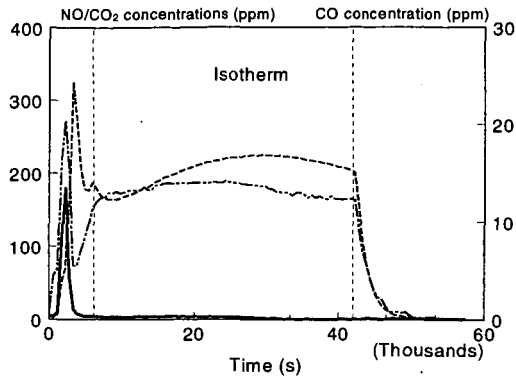


Figure 2. $\text{Cr}(\text{NO}_3)_3$ catalyzed soot oxidation. Development of NO (solid), CO_2 (dash) and CO (alternating dash) concentrations in time.

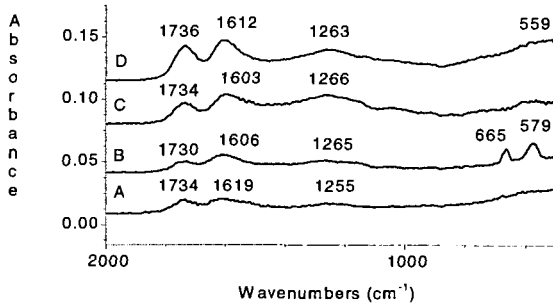


Figure 3. DRIFT spectra of partial converted soot by transition metal oxides: A. Fe_2O_3 -20%, B. Co_3O_4 -50%, C. Cr_2O_3 -20%, D. Cr_2O_3 -50%.

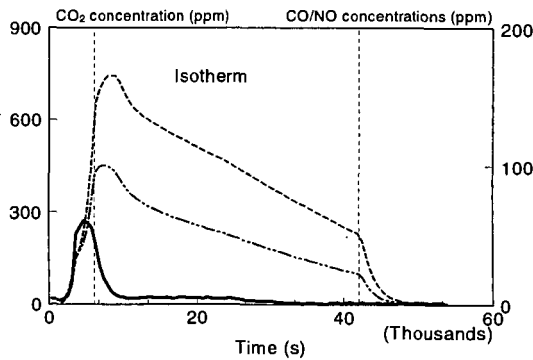


Figure 4. KNO_3 catalyzed soot oxidation. Development of NO (solid), CO_2 (dash) and CO (alternating dash) concentrations in time.

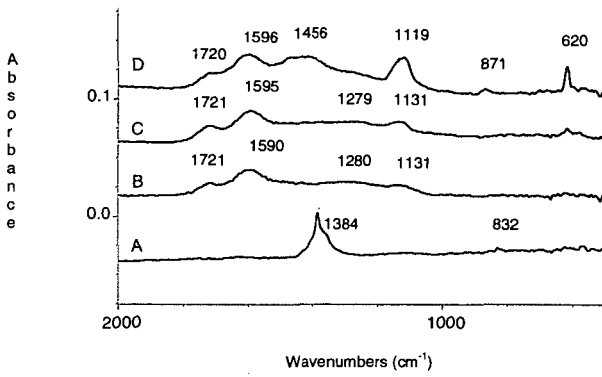


Figure 5. DRIFT spectra of partial converted KNO_3 impregnated soot : A. 0%, B. 50%, C. 75%, D. >90%

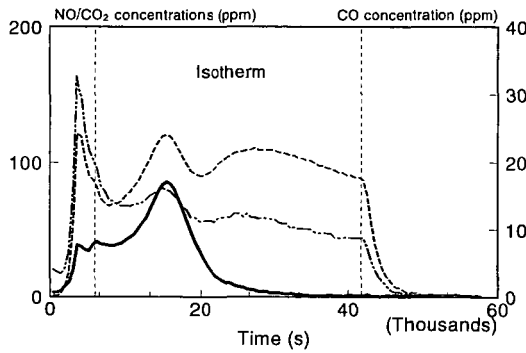


Figure 6. $\text{Ca}(\text{NO}_3)_3$ catalyzed soot oxidation. Development of NO (solid), CO_2 (dash) and CO (alternating dash) concentrations in time.

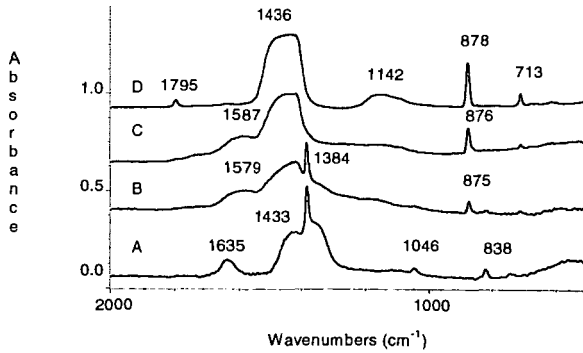


Figure 7. DRIFT spectra of partial converted $\text{Ca}(\text{NO}_3)_2$ impregnated soot : A. 0%, B. 20%, C. 50%, D. >90%

STEAM GASIFICATION OF COAL — THE EFFECTS OF ACID- AND ALKALI-LEACHING OF COAL ON ITS GASIFICATION RATE —

Satoru Murata, Akira Murakami, and Masakatsu Nomura
Department of Applied Chemistry, Faculty of Engineering, Osaka University
2-1 Yamada-oka, Suita, Osaka 565, Japan

Keywords: steam gasification, deashing, HF, HNO₃

INTRODUCTION

The conversion reaction of coal to synthesis gas (CO + H₂) is one of the most significant coal utilization processes because a wide range of coals could be applied in this process and the resulting gases are available as valuable feedstocks of chemical industry. One of the drawbacks of coal gasification is the presence of inorganic materials in coal, which cause fouling or slugging phenomena by producing scale during the gasification. Consequently, "deashing of coal" is a technically very important pretreatment for gasification. In this study we conducted acid- (HF or HNO₃) and alkali-leaching of five coals, Australian Yallourn (YL), Indonesian South Banko (SB), US Illinois NO. 6 (IL), Japanese Akabira (AK), and Australian Newstan coals (NS), the treated coals of which were submitted to steam gasification.

EXPERIMENTAL SECTION

Coal Samples

Illinois No. 6 coal was purchased from Argonne national laboratory. Newstan original and alkali-leached coals were presented by CSIRO. Other coals were our samples and stored in a glass vessel, respectively, under nitrogen atmosphere. Reagents and solvents were commercially available and used without further purification.

Leaching of coal with HNO₃

Pulverized coal (100 mesh under, 1.5 g) and 1N HNO₃ (300 mL) were stirred magnetically in a 1 L flask at 130 °C for 3 h. The products were poured into a 2 L beaker containing 100 g of ice. The resulting mixture was filtered, the filter cake being washed with water until the filtrate became neutral.

Leaching of coal with HF

A platinum crucible containing pulverized coal (100 mesh under, 2.5 g) and 46% HF (5 mL) was heated on an oil bath (90 °C) for 7 h. After the end of reaction, the resulting mixture was filtered and washed with deionized water.

Gasification reaction

Coal (ca. 10 mg, daf base) was put on a platinum cell in the heating zone of TG apparatus (Shimadzu TF-50H), being heated from room temperature to 900 °C at a heating rate of 50 K/min. Then, steam was introduced to the system at 900 °C, being kept for about 2 h. The resulting gases were analyzed by a Shimadzu GC-8A gas chromatograph (Polarpack Q column, 6mm diameter x 3m long) connected to the TG apparatus. Using the same apparatus, pyrolytic experiments were conducted for the original and treated coals (heating from room temperature to 900 °C, 5 K/min).

Heat treatment of the sample coals

The sample coals (1 g) were heated up to 900 °C with a heating rate of 30 K/min under a nitrogen stream (100 mL/min) by using an Isuzu DKRO-14K type tubular electric furnace. The resulting semicokes were submitted to specific surface area-measurement. Their specific surface area was measured by using argon adsorption method on a Shimadzu 2205 type analyzer.

RESULTS AND DISCUSSION

Deashing of the sample coals

In order to remove inorganic materials (IOM) in coal, five coals were treated by HF or HNO₃, the results being shown in Figure 1. Treatment of coal with HF resulted in removal of IOM in 36-96%, while HNO₃ treatment resulted in 33-46% removal. It should be noted that HNO₃ treatment could remove sulfur in these coals, especially, in the case of IL coal known as a high-sulfur coal, where 67% of sulfur could be removed. Huffman *et al.* had reported that sulfur in IL coal composed of 37% of inorganic form (mainly pyrite) and 63% of organic form (thiophenic and sulfidic).¹⁾ The result indicates that HNO₃-treatment could remove organic sulfur in the coal.

As to nitrogen and oxygen, N/C and O/C atomic ratios were increased by treatment with HNO₃. FT/IR spectra of the original and treated coals revealed that nitration of aromatic rings and oxidation of alkyl side chains to carboxylic groups occurred to some extent during the treatment.

Steam gasification of the original and treated coals

The original and treated coals were submitted to steam gasification. The reaction was conducted at 900 °C under steam flow (75.7 mmHg). Figure 1 shows a time profile for conversion of char. The order of gasification rate obeyed the following sequence: YL > SB > IL > NS > AK, this indicating that lower rank coals have higher reactivity than higher rank ones. These results agree well with the results reported by Hashimoto *et al.*²⁾ and Tamai *et al.*³⁾ In the case of the lower rank coals (YL and SB), HF-treatment lead to decrease their reactivity, on the other hand, HF-treatment of the higher rank coals (IL, AK, and NS) resulted in the increase of their reactivity (Figure 2). YL and SB coals contain CaO and Fe₂O₃, these are known to act as gasification catalysts. This might suggest that HF-leaching remove these catalyst species. As to HNO₃-leaching of coal, this pretreatment could improve their reactivity to a small extent (in the case of IL, AK, and NS coals). The NaOH soaked NS coal (provided by CSIRO) was found to have higher reactivity than that of the HF- or HNO₃-leached coals.

Catalytic gasification of the original and treated coals

Catalytic gasification of the sample coals was conducted. Potassium carbonate (3 wt%) was impregnated from its aqueous solution. The results of catalytic gasification are shown in Figure 3. The catalyst increased the rate of gasification as 2-4 times. In the all coals employed, HF treated coals showed higher reactivity than those of the original coals. These are different from the results of non-catalytic reaction of the lower rank coals (YL and SB).

Pyrolytic behavior of the sample coals

In order to examine the pyrolytic behavior of the sample coals, their TG/GC analyses (sample ca. 10 mg) were conducted (heating from room temperature to 900 °C at 5 K/min). TG curves are shown in Figure 4, the order of the rate of devolatilization obeying the following sequence; NS < IL < AK < SB < YL. Figure 4 also shows the time profiles for gas evolution (CO₂ and CH₄). The peak of the evolution of CO₂ was observed at 400 °C for SB and YL coals and at 700 °C for all coals, the former peak corresponding decarboxylation. On the other hand, the peak of CH₄ evolution was observed at around 600 °C. The order of its rate obeyed the following sequence; YL < SB < IL < NS < AK, this corresponding the reversed sequence for the gasification rate. Solomon *et al.* had stated that lighter hydrocarbon gas evolution during pyrolysis results in formation of crosslinking.⁴⁾ The reaction described in the following equation might occur and this might cause deactivation of char.



Specific surface area (SA) of pyrolytic residues from the sample coals was measured. SA was increased according to the sequence; IL (160 m²/g) < AK (235) < NS (275) < SB (713) < YL (870). This order does not agree with rank (carbon contents) or gasification rate of the sample coals. The lower rank coals have relatively larger SA value, this being resulted from decarboxylation reaction at around 400-500 °C.

Now, we are conducting TG/GC analyses of the acid- or alkali-leached coals and investigating a relationship between their pyrolytic behavior and reactivity.

SUMMARY

In this study, we examined the effects of acid- or alkali-leaching of five coals (from brown to bituminous coal range) on the rate of catalytic and non-catalytic steam gasification. The results obtained were summarized bellow.

- 1) HF- and NaOH-leaching of coal could remove 60-90 % of inorganic materials in it. In the case of HNO₃-leaching, degree of deashing was somewhat small, but this treatment could remove both inorganic and a part of organic sulfur.
- 2) Acid- and Alkali-leaching of coal could enhance the rate of non-catalytic and catalytic steam gasification to some extent.
- 3) TG/GC analyses of the sample coals showed the presence of some relationships between reactivity of char and amount of CH₄-evolution during pyrolysis (related to formation of cross-linking).

REFERENCES

- 1) Taghiei, M. M.; Huggins, F. E.; Shah, N.; Huffman, G. P. *Energy Fuels* 1992, 6, 293.
- 2) Hashimoto, K.; Miura, K.; Ueda, T. *Fuel*, 1986, 65, 1516.
- 3) Takarada, T.; Tamai, Y.; Tomita, A. *Fuel*, 1985, 64, 1438.
- 4) Solomon, P. R.; Fletcher, T. H.; Pugmire, R. J. *Fuel* 1993, 72, 587.

Table 1. Elemental analyses and ash contents of the original and treated coals

Samples	Atomic ratio			Ash (Wt%)	Degree of deashing (%)
	O/C	N/C	S/C		
NS coal					
Original	0.079	0.022	0.003	9.2	-
HNO ₃ -leached	0.295	0.064	0.002	6.3	33.4
NaOH-leached	0.087	0.022	0.004	0.6	93.9
HF-leached	0.102	0.021	0.003	0.4	96.4
AK coal					
Original	0.090	0.023	0.008	8.0	-
HNO ₃ -leached	0.280	0.060	0.006	4.5	46.1
HF-leached	0.101	0.023	0.008	2.7	68.8
IL coal					
Original	0.103	0.016	0.030	16.0	-
HNO ₃ -leached	0.364	0.065	0.010	8.6	50.8
HF-leached	0.150	0.016	0.025	4.7	74.3
SB coal					
Original	0.269	0.017	0.002	2.4	-
HF-leached	0.275	0.015	0.002	1.1	54.4
YL coal					
Original	0.310	0.006	0.001	1.6	-
HF-leached	0.360	0.009	0.001	1.0	36.4

Table 2. Composition of inorganic materials in the sample coals

Coals	Na ₂ O	MgO	Al ₂ O ₃	SiO ₂	CaO	Fe ₂ O ₃
NS coal	0.7	0.8	25.7	62.4	1.9	5.1
AK coal	1.6	2.0	26.1	55.2	2.2	6.7
IL coal	0.9	0.7	19.4	35.4	10.0	27.3
SB coal	1.3	2.1	20.0	12.8	16.6	11.5
YL coal	6.0	19.5	1.4	12.6	14.4	33.6

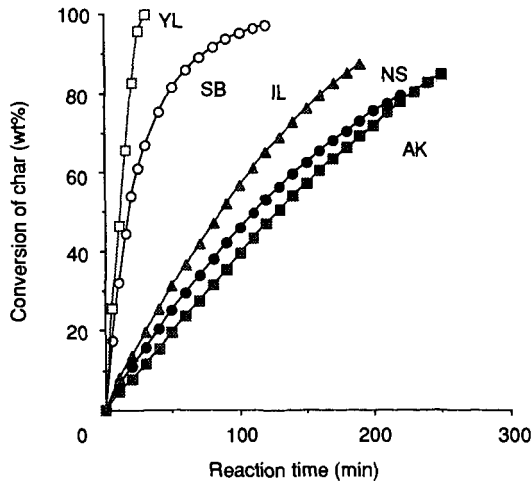


Figure 1. Time profile of steam gasification of sample coals

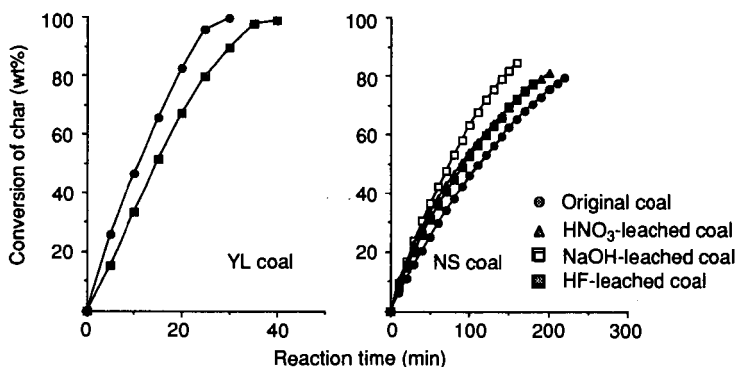


Figure 2. Steam gasification of the original and treated coals
Catalyst K₂CO₃ 3wt%, 1173 K, steam flow

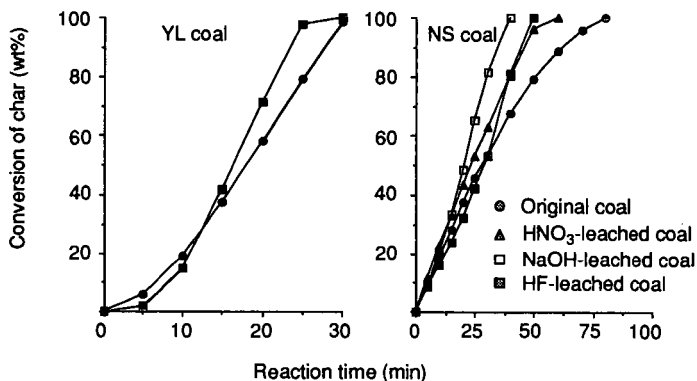


Figure 3. Catalytic gasification of the original and treated coals
Catalyst K₂CO₃ 3wt%, 1173 K, steam flow

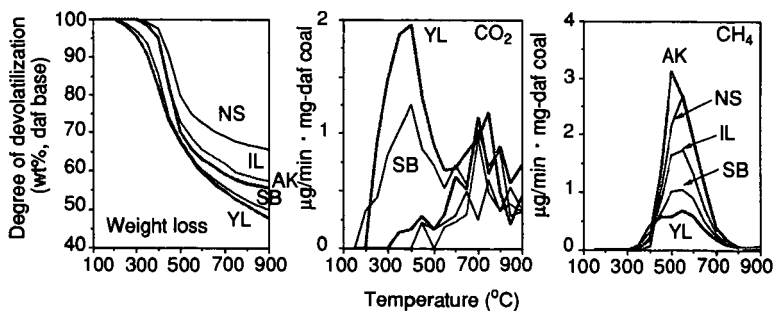


Figure 4. TG/GC analyses of the sample coals